buildings

MDPI

Article

Behaviour of Lightweight Concrete Wall Panel under Axial Loading: Experimental and Numerical Investigation toward Sustainability in Construction Industry

Muhammad Ekhlasur Rahman [1,2,*], Timothy Zhi Hong Ting [2], Hieng Ho Lau [2,3], Brabha Nagaratnam [1] and Keerthan Poologanathan [1]

[1] Department of Mechanical and Construction Engineering, University of Northumbria, Newcastle upon Tyne NE7 7YT, UK; brabha.nagaratnam@northumbria.ac.uk (B.N.); keerthan.poologanathan@northumbria.ac.uk (K.P.)
[2] Department of Civil & Construction Engineering, Faculty of Engineering and Science, Curtin University Malaysia, Miri 98009, Malaysia; timothy.ting@curtin.edu.my (T.Z.H.T.); hhlau@swinburne.edu.my (H.H.L.)
[3] Faculty of Engineering, Computing and Science, Swinburne University of Technology, Miri 93350, Malaysia
* Correspondence: muhammad2.rahman@northumbria.ac.uk

Abstract: Awareness of sustainability in construction has led to the utilization of waste material such as oil palm shell (OPS) in concrete production. The feasibility of OPS as alternative aggregates in concrete has been widely studied at the material level. Meanwhile, nonlinear concrete material properties are not taken into account in the conventional concrete wall design equations, resulting in underestimation of lightweight concrete's wall axial capacity. Against these sustainability and technical contexts, this research investigated the buckling behavior of OPS-based lightweight self-compacting concrete (LWSCC) wall. Failure mode, load-deflection responses, and ultimate strength were assessed experimentally. Numerical models have been developed and validated against experimental results. Parametric studies were conducted to study the influence of parameters like slenderness ratio, eccentricity, compressive strength, and elastic modulus. The results showed that the axial strength of concrete wall was very much dependent on these parameters. A generalized semi-empirical design equation, based on equivalent concrete stress block and modified by mathematical regression, has been proposed. The ratio of average calculated results to test results of the proposed equation, when compared to ACI 318, AS 3600, and Eurocode 2 equations, are respectively improved from 0.36, 0.31, and 0.42 to 0.97. This research demonstrates that OPS-based LWSCC concrete can be used for structural axial components and that the equation developed can serve a good guideline for its design, which could encourage automation and promote sustainability in the construction industry.

Keywords: oil palm shell; compressive strength; concrete wall; elastic modulus; eccentricity; slenderness ratio

Citation: Rahman, M.E.; Ting, T.Z.H.; Lau, H.H.; Nagaratnam, B.; Poologanathan, K. Behaviour of Lightweight Concrete Wall Panel under Axial Loading: Experimental and Numerical Investigation toward Sustainability in Construction Industry. *Buildings* **2021**, *11*, 620. https://doi.org/10.3390/buildings11120620

Academic Editor: Francisco López Almansa

Received: 13 November 2021
Accepted: 29 November 2021
Published: 6 December 2021

1. Introduction

1.1. Sustainable Aspect of Agricultural Waste

Concrete is undoubtedly one of most consumed construction materials worldwide. Since aggregates constitutes about 65% to 80% of total concrete volume [1], this heavy consumption has led to gradual exhaustion of conventional resources for aggregate production. This has created the need for more sustainable and economical alternative aggregate materials. Reusing of recycled aggregate or waste material can be regarded as a promising approach [2]. However, due to further processing of recycled aggregate [3] and durability-related issue [4,5], the use of recycled aggregate is not favourable. Alternatively, normal-weight aggregates (NWA) in concrete production can be replaced with other materials, such as lightweight aggregates (LWA), which are either natural or generated by-products

from industrial or agricultural processing. LWA can generally be categorized as natural form or artificial type, with artificial type being the most commonly used as an alternative aggregate in concrete by researchers [3,6,7]. The use of waste materials as LWA can minimize the depletion of natural resources while promoting the proper management of solid waste [8]. Oil palm shell, an agricultural waste generated from the oil palm industry, is abundantly available in countries such as Malaysia, Indonesia, Thailand, and Nigeria [9]. Oil palm mills generate massive amount of OPS, with over 4 million tonnes being produced annually [6,10,11]. The waste management issues are becoming more challenging as the generation of oil palm solid wastes increases. As such, there is a great urgency to carry out more research into utilizing OPS in order to reduce environmental impacts associated with agricultural waste treatment and disposal [12–14].

The application of lightweight aggregate concrete (LWAC) as a building material in industrial construction has been extensively promoted since the 1960s due to its lightweight characteristics [15]. An innovative construction material, especially when incorporated with environmentally friendly constituents, lightweight self-compacting concrete (LWSCC) has emerged as a superior construction material since 1992 [3], with its advantageous properties, including self-compacting ability, lower density, improved thermal conductivity, and comparable compressive strength to normal concrete. Most important of all, it is a more sustainable material, particularly if designed with OPS aggregates. Furthermore, LWSCC is more favorable in large complex structural applications, particularly in tall buildings or long-span structures.

1.2. Research on OPS Concrete

Research [13,16–18] has shown that OPS has an enormous potential to be an alternative LWA in concrete production due to its low density and reasonable compressive strength. Generally, the compressive strength of OPS concrete ranges from 20 to 35 MPa [9,13,19–21]. Compressive strength of more than 50 MPa has been reported by several researchers [17,18,22,23]. In terms of splitting tensile strength of OPS concrete, some research [18,24,25] has revealed that the value of splitting tensile strength possessed by OPS concrete is approximately 6–10% of its compressive strength. As for water absorption, Teo, Mannan, Kurian and Ganapathy [16] observed that the water absorption of OPS-based concrete is 11.23% for air-dry curing and 10.64% for full-water-submerged curing. According to Shafigh, Jumaat and Mahmud [17], the water absorption of OPS concrete ranges between 3 and 6%, which, being less than 10%, means that it may be considered good concrete. Despite significant research on the compressive strength of OPS-based concrete at the material level, there is limited research on the use of OPS-based concrete as a vertical structural component, such as a column and wall, where buckling can be the main concern for slender components. There is insufficient knowledge on the buckling behaviour of OPS-based concrete to be used as a load-bearing component for practicing engineers, and therefore it is crucial to investigate the buckling behaviour of OPS-based concrete.

1.3. Concrete Wall Subjected to Axial Loading

A concrete wall panel can be designed as a load-bearing wall if it only resists vertical loading without being subjected to bending. The concrete wall panel under axial loading in an idealized condition generally behaves as a one-way wall with hinged condition at both the top and bottom and with free vertical edges [26]. A uniaxial curvature in the direction of loading can develop. Since the thickness of concrete wall panel is smaller than the other dimensions [27], a slenderness effect is introduced. Slenderness ratio is defined as the ratio of height to thickness of the wall. The behaviour of wall panels under axial loading can vary substantially from short and wide to deep and narrow slender members [28]. Similar to the column, the failure mode of the wall panel under axial loading is highly dependent on the slenderness ratio [29,30], where a small slenderness ratio can cause crushing failure, while a high slenderness ratio leads to buckling failure. The ultimate load-bearing capacity of the wall panel is greatly affected by the slenderness ratio.

1.4. Design Guide and Research of Concrete Wall

At present, standards such as the American Concrete Institute (ACI 318) standard [31], the Australian Standard (AS 3600) [32], and Eurocode 2 [33] provide simplified equations for determining the load-bearing capacity of the concrete wall panel. According to several researchers, the design equation provided by the ACI standard is conservative [34–37]. Due to its over-simplicity, this equation is not able to account for the material and geometric nonlinearity in the buckling failure of a slender concrete wall panel [34,38]. In the ACI equation, it is assumed that the load is applied within t/6 of the concrete cross-section, whilst the eccentricity component is not considered. The equation is the product of f′c, cross-sectional area, and slenderness ratio parameter. The ACI standard specified a modification factor to consider the effect of lightweight-aggregates-based concrete. However, this factor has not been included in the existing wall design equation. As for AS 3600 and Eurocode 2, the eccentricity parameter is considered. However, the effects of material nonlinearity, including nonlinear increment of compressive strength and elastic modulus, which are responsible for buckling, are not taken into consideration. In order to predict the strength of slender lightweight wall more accurately, all the aforementioned parameters must be considered. The alternative column design approach in ACI 318 and AS 3600 can be used to determine the axial strength of wall by treating one-way wall as column. The effective rigidity approach was adopted in ACI 318, and rigidity of the section under balanced failure was used in AS3600. Oberlender [39] mentioned that the column approach can yield better prediction compared to a simplified design equation. However, more recent research [37] showed that the column design approach is less accurate for slender wall. This is because the standards ignored the effect of load eccentricity in determining the effective rigidity for buckling load. Similarly, the effect of material nonlinearity is not considered.

Research on the buckling behaviour and design equation of concrete load-bearing wall has been conducted over the past 60 years. In earlier years, Seddon [40] studied the behaviour of normal concrete wall under concentric and eccentric loadings in one-way action with a slenderness ratio varied from 18 to 54. The author noticed that concrete wall panel failed by crushing for slenderness ratios of less than 20, while buckling failure was noticed for slenderness ratios of more than 20. However, the author noticed that there was no significant strength reduction due to buckling instead of crushing. Oberlender [39] conducted a comprehensive study on 54 normal concrete wall panels with slenderness ratios varying from 8 to 28 and aspect ratios from 1 to 3.5. Similarly, the authors noticed a crushing failure for wall panels with slenderness ratios of less than 20, while buckling failure was observed for a slenderness ratio of 28. For slenderness ratios of 20 and 24, combinations of crushing and slight buckling were observed. A similar observation was noted by subsequent researchers [28,41,42]. Saheb and Desayi [28] modified the design equation of ACI 318 by incorporating the aspect ratio component. Meanwhile, Fragomeni and Mendis [35] performed a series of studies on normal and high-strength concrete wall panels with slenderness ratios varying from 12 to 25. The authors concluded, by comparing normal-strength and high-strength wall panels of the same dimensions, that high-strength concrete wall panel exhibited more brittle failure under one-way action. The authors also claimed that the ultimate strength of reinforced concrete wall panel under axial loading is governed by the nonlinear concrete compressive strength. The authors modified the design equation of AS 3600 by including high-strength concrete parameters. The findings of Fragomeni and Mendis [35] were further confirmed by Doh and Fragomeni [43] with wall slenderness ratios varying from 25 to 40. Doh and Fragomeni [43] further modified the design equation [35] by modifying the compressive strength component with an order of 0.7 to account for the nonlinear strength effect.

For more recent research, Ganesan, Indira and Prasad [30] investigated the behavior of steel-fiber-reinforced self-compacting concrete (SFRSCC) and steel-fiber-reinforced concrete (SFRC) wall panels in one-way action with slenderness ratios of 12 to 30. The authors concluded that the inclusion of steel fibers were able to improve the cracking behavior and ductility of concrete wall. The effects of slenderness ratio and aspect ratio were similar

to the normal type of concrete wall. Meanwhile, Ganesan, Indira and Santhakumar [36] conducted a series of tests on reinforced normal concrete and geopolymer concrete wall panels. The authors noticed that for the same wall geometry, geopolymer concrete wall panel exhibited more softening behavior when compared to normal concrete wall panel. Normal concrete wall panel displayed steeper slope in load versus lateral deflection when compared to the geopolymer concrete wall panel. The authors explained that the content of finer particles in the matrix of geopolymer concrete resulted in more ductile behavior. Both studies [30,36] modified the factor and slenderness ratio component of the ACI 318 equation to account for the effects of different types of concrete including steel-fiber-reinforced self-compacting concrete (SFRSCC), steel-fiber-reinforced concrete (SFRC), and geopolymer concrete, respectively. On the other hand, Huang, Hamed, Chang and Foster [37] performed a series of experimental and numerical studies on the load-bearing capacity of high-strength concrete wall panels. The authors concluded that the column design approach and simplified wall design equations in design standards could not accurately estimate the axial capacity of slender wall. This is mainly because the effects of geometrical and material nonlinearity are not considered in either the column design approach or the simplified design standard equation. It is obvious that researchers have concentrated on modifying the factors to account for the geometric effects, which are slenderness ratio and aspect ratio. However, it is obvious that these simplified equations have not taken into consideration all of the material nonlinearity effects, such as compressive strength and elastic modulus of concrete.

1.5. Research Significance

Generally, the use of lightweight aggregates in concrete will significantly reduce its elastic modulus. Several researchers [44–46] have shown that for a given compressive strength, lightweight concrete exhibits more ductile stress-strain behavior under compression loading compared to normal-weight concrete. By using concrete with a lower elastic modulus value as material in slender wall, lightweight concrete wall tends to have a lower ultimate axial capacity. According to the Euler buckling theorem [47,48], the buckling load is a function of the elastic modulus. However, all the current equations [28,30–33,39,41–43,49–51] are expressed as a function of concrete compressive strength and wall cross-sectional area only. Without considering the elastic modulus parameter, this can lead to unsafe prediction of the ultimate axial capacity of the lightweight concrete wall under eccentric loading. Thus, it is necessary to propose a new design equation that can enhance the confidence of utilizing agricultural-waste-incorporated lightweight concrete as structural wall for practical engineers to promote sustainability.

1.6. Objective

Based on the extensive literature review undertaken, research tends to focus on normal and high-strength concrete wall panels rather than those cast from lightweight concrete. More comprehensive research in lightweight concrete wall is important in order to gain an insight into the subject. Thus, the aim of this research is to investigate the buckling behavior of OPS-based LWSCC wall subjected to axial loading. An experimental study was carried out on axially loaded slender, lightweight, self-compacting concrete wall panels with different configurations to investigate the structural behavior and performance. FEA models were constructed using ABAQUS 6.14 and validated against both experimental results and published data. Using the validated models, parametric studies were then carried out on the effects of eccentricity, slenderness ratio, compressive strength, and elastic modulus of lightweight concrete wall. Finally, a semi-empirical design equation for slender wall for evaluating the axial load-bearing capacity of concrete wall panel was proposed and further validated against published data.

2. Experimental Program

2.1. Materials

Grade 45 Ordinary Portland Cement (OPC) and Class F low-calcium fly ash, which conform to ASTM: C150/C150M-12 [52] and ASTM C618 [53], respectively, were used as binder. The chemical properties are shown in Table 1. Oil palm shell (OPS), as shown in Figure 1, supplied by an oil palm processing mill in Miri, Sarawak, Malaysia, was used as coarse aggregates in the mix design. The specific gravity and water absorption of the river sand and OPS aggregate used are summarized in Table 2. The particle size of the aggregates is shown in Figure 2. A lightweight self-compacting concrete (LWSCC) obtained from particle-packing method was used for casting test specimens. The mix design and same materials source from previous research [54] were used, and they are summarized in Table 3. Concrete cylinders with a diameter of 100 mm and a height of 200 mm were cast and cured along with wall specimens. Six test cylinders each were prepared for both compressive and splitting tensile tests, and in every batch, uniaxial compression tests [55] were carried out to determine the compressive strength and corresponding stress-strain behavior. Splitting tensile tests [56] were performed to determine the splitting tensile strength of the concrete. Compressive and splitting tensile strengths are presented in Table 4.

Table 1. Chemical properties of cement and fly ash [54].

Chemicals	Cement (%)	Fly Ash (%)
Silicon dioxide (SiO_2)	20.0	57.8
Aluminium oxide (Al_2O_3)	5.2	20.0
Ferric oxide (Fe_2O_3)	3.3	11.7
Calcium oxide (CaO)	63.2	3.28
Magnesium oxide (MgO)	0.8	1.95
Sulfur trioxide (SiO_3)	2.4	0.08
K_2O	-	3.88
TiO_2	-	2.02
Na_2O	-	0.30
Loss on ignition	2.5	0.32

Figure 1. Oil palm shell aggregates.

Table 2. Physical properties of aggregates [54].

Physical Property	River Sand	OPS
Specific gravity	2.64	1.19
Water absorption (24 h) (%)	1.1	18.11
Aggregate impact value (AIV) (%)	-	4.2

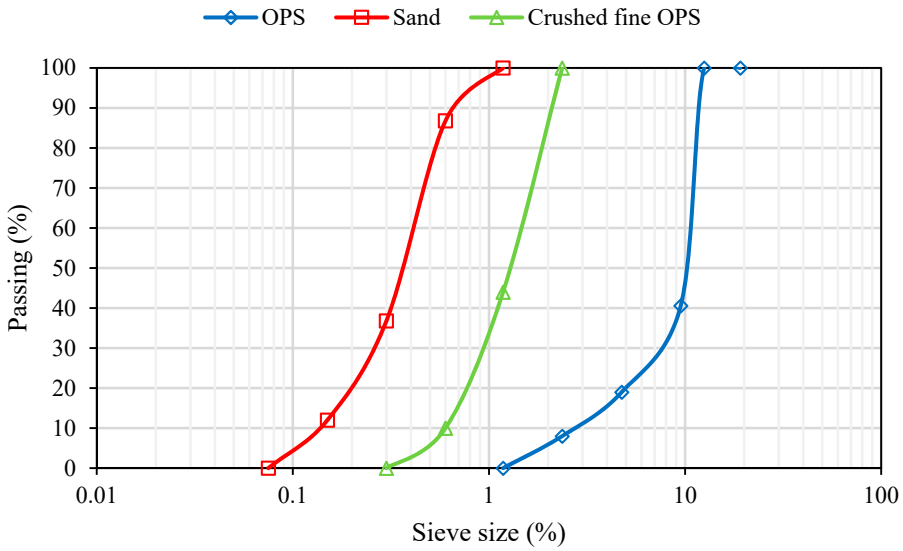

Figure 2. Particle size distribution of OPS and river sand [54].

Table 3. Concrete mix design [54].

Cement (kg/m^3)	Fly Ash (kg/m^3)	Water (kg/m^3)	Sand (kg/m^3)	OPS Aggregate (kg/m^3)	SP (kg/m^3)
312	208	161.2	715	455	8.6

Table 4. Specimen dimensions and strengths.

Specimen	Height L (mm)	Width W (mm)	Thickness t (mm)	Average Compressive Strength (MPa)	Average Splitting Tensile Strength (MPa)	Nominal Density (kg/m^3)
T25-AR1.8SR17 [a]	425	235	25	16.4	1.5	1829
T25-AR1.8SR23 [a]	565	315	25			
T25-AR3.1SR23 [a]	565	185	25			
T25-AR5.3SR23 [a]	565	105	25			
T60-AR5.3SR23 [b]	1400	260	60	13.7	1.1	1823

Note: [a] T25 series specimens were from 1st batch of concrete. [b] T60 series specimens were from 2nd batch of concrete.

2.2. Wall Specimens

For wall panel with a thickness of 60 mm, slender wall panels were designed with slenderness ratio of 23 and aspect ratio of 5.3. In the case of wall specimens with a thickness of 25 mm, the slenderness ratio ranged from 17 to 23, and the aspect ratio ranged from 1.7 to 5.3. According to ACI and AS, a minimum reinforcement ratio of 0.0015 must be provided to prevent cracking of concrete due to thermal stress. Reinforcement ratios of 0.0058 and 0.003 were provided for the vertical and horizontal direction, respectively. For the wall specimen of 60 mm thickness, grade 300 steel mesh with a diameter of 5 mm and a spacing of 200 mm was used. Two layers of steel mesh were used with concrete cover of 15 mm and 30 mm c/c spacing between two meshes. A single layer of steel reinforcement was used for the 25 mm thickness series. The 25 mm thickness wall specimens were reinforced by steel bar with diameter ranging from 3 to 4 mm. The reinforcement ratios of 0.0058 and 0.003 were provided for the vertical and horizontal direction, respectively, in order to fulfil the minimum reinforcement requirement specified in ACI and AS3600. Three specimens were prepared and tested for each configuration. Typical dimensions of the specimens are illustrated in Figure 3. The dimensions and concrete strengths of hardened wall specimens were presented in Table 4. As for the specimen naming scheme, the abbreviations 'T', "A", and "SR" indicate thickness, aspect ratio, and slenderness ratio of specimen, respectively. During the first seven days after casting, a wet cotton cloth was put on the surface of the

specimen and covered with plastic. Water was continually applied to preserve the moisture of the cloth. After removal of the formwork, all the specimens were fully wrapped in plastic and moisturized until the day of testing.

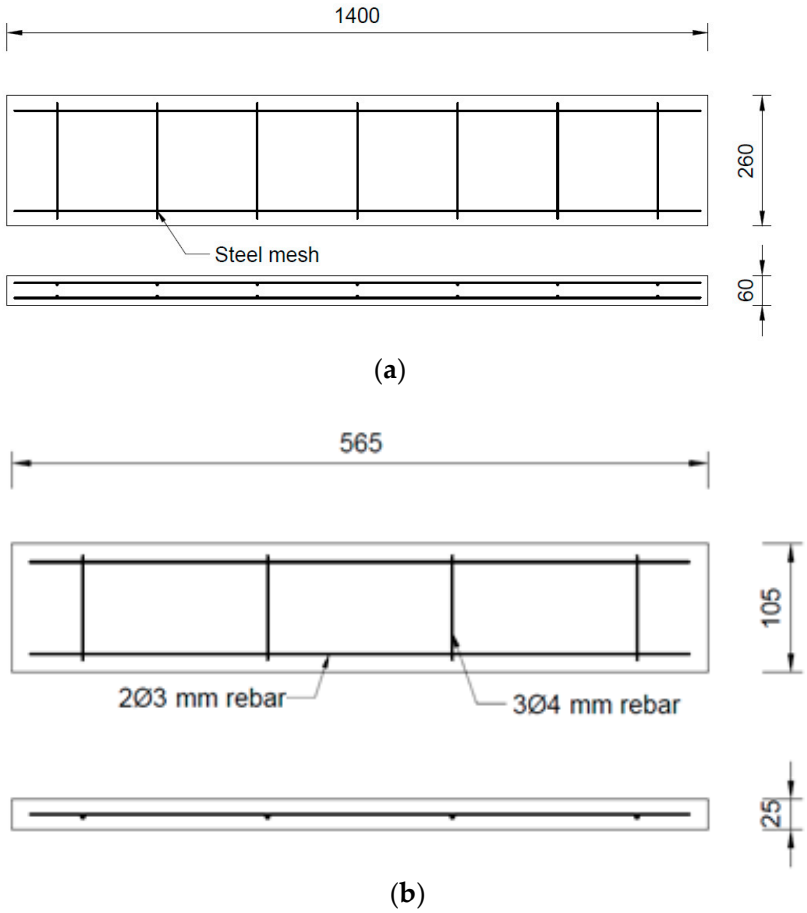

Figure 3. Specimen layout: (**a**) T60-AR5.3SR23, (**b**) T25-AR5.3SR23.

2.3. Experimental Setup and Instrumentation

All wall panels were tested with pinned connection at both the top- and bottom-end supports. Lotus Hydraulic Jack was used to transfer uniform load through a spreader beam as a concentric load for T60 series specimen. Gotech universal testing machine was used for T25 series. For loading procedure, the wall specimens were pre-loaded to 1 kN to check and confirm that all the instruments were in working condition and to eliminate the gaps. The load was then increased gradually until the specimen failed. Linear Variable Displacement Transducers (LVDT) were mounted at a quarter height, mid height, and third-quarter height of the wall to measure the horizontal displacement for wall specimen with 60 mm thickness. For wall specimens with 25 mm thickness, LVDT was only mounted at mid height due to limited space. TML Data Logger TPS 530 was used to record the loading and displacement data. The support condition detail is shown in Figure 4. The behavior of the specimens was observed and recorded throughout the tests.

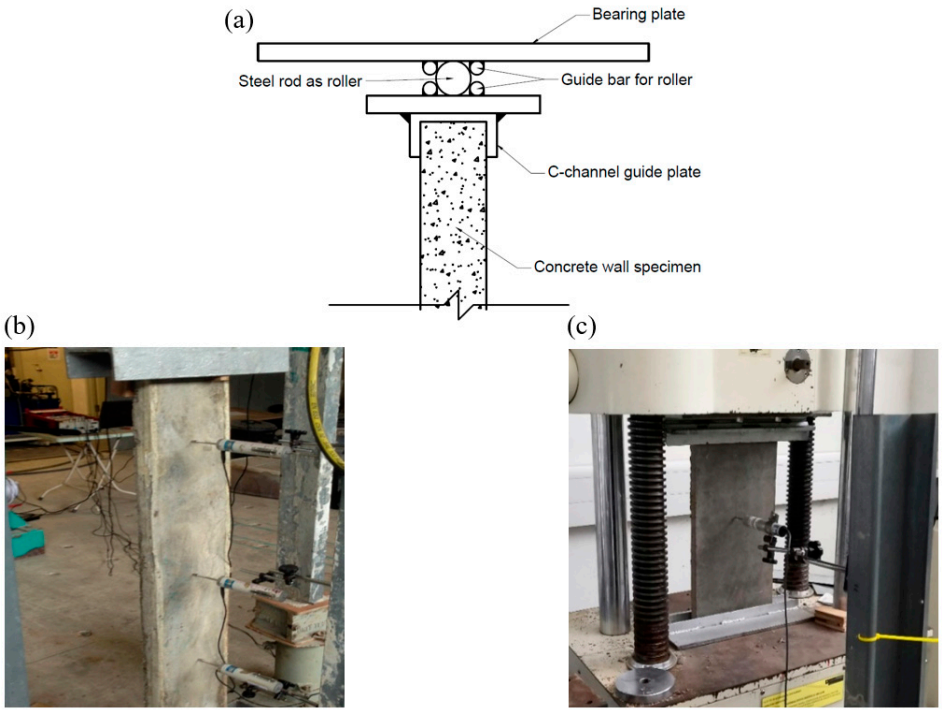

Figure 4. Detail of support condition: (**a**) Schematic diagram, (**b**) Experimental setup for T60 series, (**c**) Experimental setup for T25 series.

3. Finite Element Model

3.1. Material Model of Concrete

A constitutive model based on a combination of damage mechanics and plasticity, Concrete Damaged Plasticity (CDP), is used to model the concrete material of wall under axial loading. The elastic modulus of concrete is defined in accordance with the recommendation provided in AS 3600, and given as Equations (1) and (2). The compressive stress-strain model of Yang, et al. [57] is represented by a parabola with peak stress at its vertex. The peak strain which corresponds to the peak stress is given by Equation (3). The strain that correlates with 50% of the peak stress in the descending branch is given by Equation (4). The stress-strain relationship of concrete is represented by Equation (5). This model is pertinent to concrete with compressive strength ranging from 10 to 180 MPa and density from 1200 to 4500 kg/m^3. The β_1 parameters of ascending and descending branches are determined from Equations (6) and (7), respectively. The comparison of stress-strain curves determined from the experimental test and the empirical model is shown in Figure 5a. The curve computed from the empirical model is close to the experimental. This confirmed that the empirical model is able to capture the actual stress-strain behavior of OPS based lightweight self-compacting concrete. Thus, this empirical stress-strain model was used for the parametric study of wall with varying compressive strength and elastic modulus. For the compressive stress strain input in CDP, the total strains of the raw stress-strain curve are converted into inelastic strain [58] by using Equation (9), and these are shown in Figure 5a. In addition, the compression damage parameters [58] are determined by using Equation (10). Five parameters comprising dilation angle, eccentricity, σ_{b0}/σ_{c0} ratio, K_c, and viscosity are required to be inputted in the CDP model. The parameters used are summarized in Table 5.

$$E_c = \rho^{1.5}\left(0.043\sqrt{f'_c}\right) \text{ for } f'_c \leq 40 \text{ MPa} \quad (1)$$

$$E_c = \rho^{1.5}\left(0.024\sqrt{f'_c + 0.12}\right) \text{ for } f'_c > 40 \text{ MPa} \quad (2)$$

where E_c is the elastic modulus of concrete; ρ is the concrete density; and f'_c is the cylinder compressive strength.

$$\varepsilon_0 = 0.0016e^{240\frac{f'_c}{E_c}} \tag{3}$$

$$\varepsilon_{0.5} = 0.0035e^{1.2\{(\frac{10}{f'_c})(\frac{w_c}{2300})\}^{1.75}} \tag{4}$$

$$f_c = \left[\frac{(\beta_1+1)\left(\frac{\varepsilon_c}{\varepsilon_0}\right)}{\left(\frac{\varepsilon_c}{\varepsilon_0}\right)^{\beta_1+1}+\beta_1}\right] f'_c \tag{5}$$

$$\beta_1 = 0.2e^{0.73\xi}, \; for \; \varepsilon_c \leq \varepsilon_0 \tag{6}$$

$$\beta_1 = 0.41e^{0.77\xi}, \; for \; \varepsilon_c > \varepsilon_0 \tag{7}$$

$$\xi = \left(\frac{f'_c}{10}\right)^{0.67}\left(\frac{2300}{w_c}\right)^{1.17} \tag{8}$$

where ε_0 is the concrete strain corresponding to ultimate compressive stress; $\varepsilon_{0.5}$ is the strain that correlates with the 50% of peak stress in the descending branch; f_c is the compressive stress at some point in the stress strain curve; w_c is the weight of LWSCC; β_1 is the parameter for the ascending and descending branch of the stress strain curve; ε_c is the concrete strain; and ξ is the constant parameter.

$$\varepsilon_i = \varepsilon_{c.t} - \frac{\sigma_c}{E_c} \tag{9}$$

$$d_c = 1 - \frac{\sigma_c}{\sigma_{max}} \tag{10}$$

where ε_i is the inelastic tensile strain; $\varepsilon_{c.t}$ is the total compressive strain; σ_c is the corresponding compressive stress; d_c is the compressive damage parameter; and σ_{max} is the ultimate compressive stress.

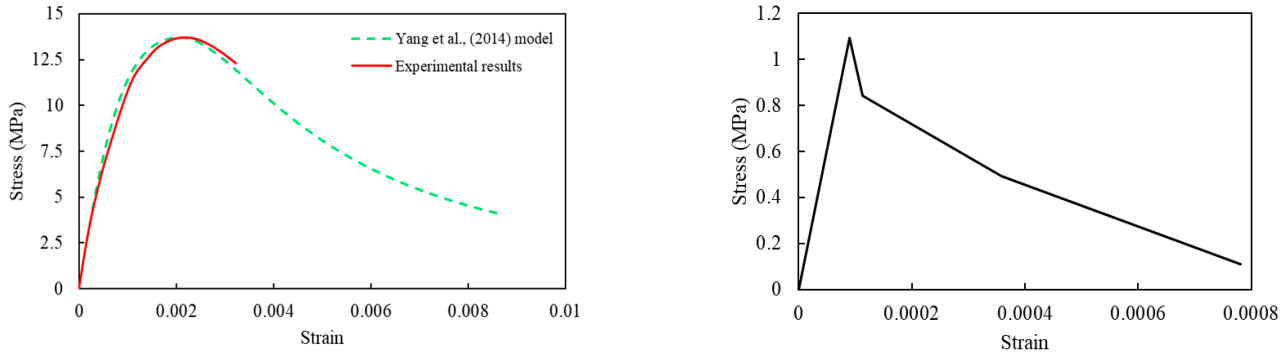

(**a**) (**b**)

Figure 5. Stress versus inelastic strain: (**a**) compressive, (**b**) tensile.

In ABAQUS, the uniaxial tension properties of concrete are required in the CDP model. In order to obtain the uniaxial tensile strength of lightweight concrete, the splitting tensile strength is determined through laboratory test. It was then converted into uniaxial tensile strength by using Equation (11) from the guidelines of AS 3600. The tension stiffening model of Wahalathantri, et al. [59] has been chosen in this research. This model was originally proposed by Hillerborg, et al. [60] and modified by Nayal and Rasheed [61] to avoid discontinuity in global response. The model of Nayal and Rasheed [61] comprises of two regions, which are primary and secondary cracking stages. The model was then modified by Wahalathantri, Thambiratnam, Chan and Fawzia [59] to avoid runtime errors in ABAQUS. The critical tensile strain is calculated from uniaxial tensile strength using Equation (12), and the resulting stress-strain curve is shown in Figure 5b. For CDP tensile

stress-strain input, the total strains of the raw stress-strain curve are converted to inelastic strain using Equation (13). In addition, the compression damage parameters are determined by using Equation (14).

$$\sigma_{ct} = 0.9 f_{ct.sp} \tag{11}$$

$$\varepsilon_{t.cr} = \frac{\sigma_{ct}}{E_c} \tag{12}$$

$$\varepsilon_t^{ck} = \varepsilon_{t.cr} - \frac{\sigma_t}{E_c} \tag{13}$$

$$d_t = 1 - \frac{\sigma_t}{\sigma_{t.max}} \tag{14}$$

where σ_{ct} is the uniaxial tensile stress; $f_{ct.sp}$ is the experimental splitting tensile stress; $\varepsilon_{t.cr}$ is the critical tensile strain; ε_t^{ck} is the inelastic tensile train; σ_t is the corresponding tensile stress; d_t is the tensile damage parameter; and $\sigma_{t.max}$ is the ultimate tensile stress.

Table 5. Input parameters for CDP.

Parameters	Values
Elastic modulus (MPa)	12,047
Poisson ratio	0.2
Density (kg/m^3)	1800
Dilation angle	31°
Eccentricity	0.1
Initial biaxial/uniaxial ratio, σ_{c0}/σ_{b0}	1.16
K_c	0.667
Viscosity	0.001

3.2. Material Model of Steel

A bilinear stress-strain relation was adopted for steel reinforcement. The engineering stresses determined in the laboratory test are converted into true stresses by using Equation (15). True strains are determined from engineering strain by using Equation (16). The inputs are summarized in Table 6.

$$\sigma_{true} = \sigma(1 + \varepsilon_{eng}) \tag{15}$$

$$\varepsilon_{plastic}^{pl} = ln(1 + \varepsilon_{eng}) - \frac{\sigma}{E_s} \tag{16}$$

where σ_{true} is the true stress; ε_{eng} is the engineering strain; E_s is the elastic modulus of steel; and $\varepsilon_{plastic}^{pl}$ is the plastic strain.

Table 6. Material properties of steel.

Fsy (MPa)	Fsu (MPa)	v
299	374	0.3

3.3. Model Description

The quasi-static analysis of implicit solver in ABAQUS/Standard was chosen for modelling. A three dimensional 8-node brick element with reduced integration, C3D8R, was used to model concrete, while steel reinforcement was modelled with three-dimensional two-node straight truss element, T3D2. The interaction between concrete and reinforcing steel bars was modelled using the "Embedded Region" constraint in ABAQUS. This is a common method for defining the interaction of reinforcing steel in concrete [62]. Both ends of the concrete wall were modelled as pinned end conditions to simulate the actual support conditions of the laboratory test. All the boundary conditions and applied loads were specified at the respective reference points. Reference points (RP) were created

at both ends. The loading was applied in the form of imposed displacement by using smooth step amplitude function at the reference point. Suitable mesh size was determined through a mesh convergence study to provide a good balance between accuracy and computational efficiency.

3.4. Summary

The overview of experimental and FEA modelling methods is provided in Figure 6 for clarity.

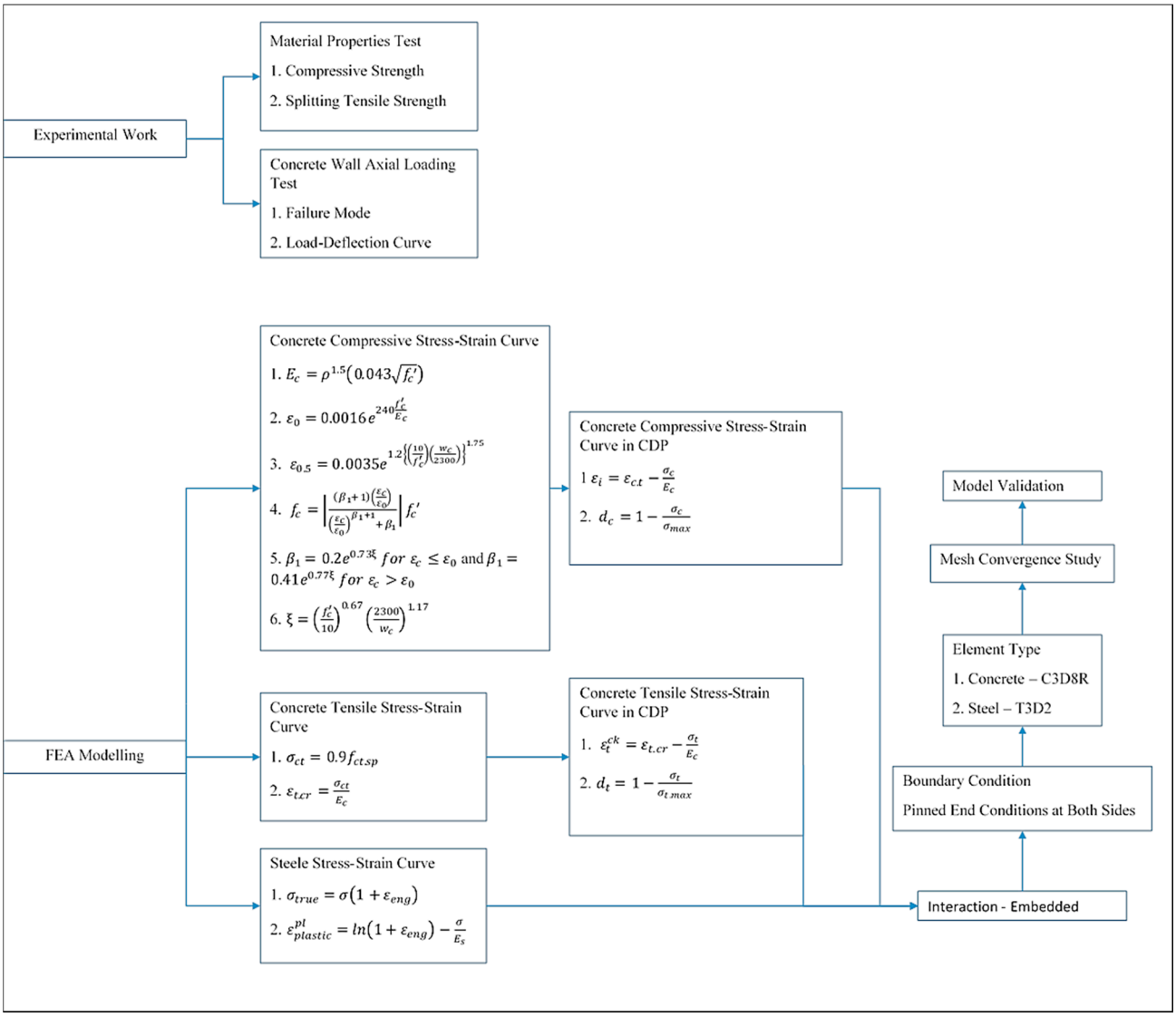

Figure 6. Overview of research methodology.

4. Results and Discussion

4.1. Experimental Results and Analysis

Experimental outcomes, including failure mode, failure load, and load-deflection, are discussed and used to evaluate the axial behavior of lightweight concrete wall panels.

4.1.1. Failure Mode

The failure characteristics of T60 series wall specimen is shown in Figure 7a. A large horizontal crack was noticed on both sides of the wall panel near the center. T60-AR5.3SR23 specimen failed predominantly by buckling in a single curvature shape with maximum

deflection at the center. The slenderness ratio of the specimen was 23 and was considered to be slender wall since it bended at mid height. This is in good agreement with the findings of Fragomeni and Mendis [35], in which concrete walls with a slenderness ratio equal to or greater than 20 could commonly fail by buckling with horizontal cracks at mid height.

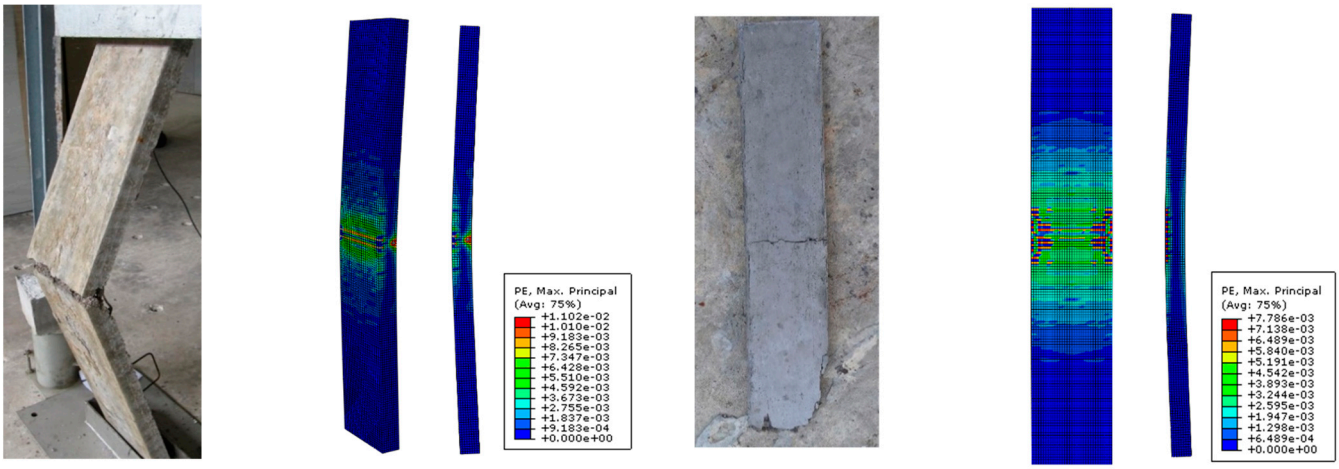

(**a**) (**b**)

Figure 7. Comparison between experimental and FEA failure mode (**a**) T60-AR5.3SR23, (**b**) T25 AR5.3SR23.

The failure modes of T25 series specimens are shown in Figure 7b. Specimen T25-AR1.8SR17, T25-AR1.8SR23, T25-AR3.1SR23, and T25-AR5.3SR23 failed by buckling at mid height. The slenderness ratios of these specimens ranged from 17 to 23. Similarly, horizontal crack near the wall center as well as some cracks near the support ends were also observed for these specimens. These specimens failed predominately by buckling, since an obvious curvature shape with significant cracking at mid height were observed when they failed. This study shows good agreement with the findings of Oberlender [39] and Saheb and Desayi [28] that the concrete wall with high slenderness ratio failed by buckling at mid height.

4.1.2. Load Deflection

The axial load versus lateral deflection gives the structural deformation response of concrete wall under loading. Figure 8a shows the load versus lateral deflection profile of wall at top-quarter, mid, and bottom-quarter height, respectively, for specimen T60-AR5.3SR23, while Figure 8b,c illustrate the load versus lateral deflection curve at mid height for T25 series specimens. These curves show that the concrete wall specimens exhibit ductile behavior with continuous increasing of lateral deflection with increasing load. The curves show linear behavior in the initial loading region, which is followed by nonlinear curve up to the ultimate failure load. The curves show that only slight deflection is produced with increasing load in the linear region, and the linearity is about 45–55% of ultimate failure load. In the nonlinear region, the lateral deflection increases rapidly as the load is increased. As shown in Figure 8a, specimen T60-AR5.3SR23 has a maximum deflection of 7 mm at mid height and roughly 5 mm at both quarter heights. The deflection profile of specimens show fairly uniform curvature along the height with maximum deflection at mid height. In short, the curves show that OPS-based LWSCC wall exhibits fairly ductile load-deflection behavior.

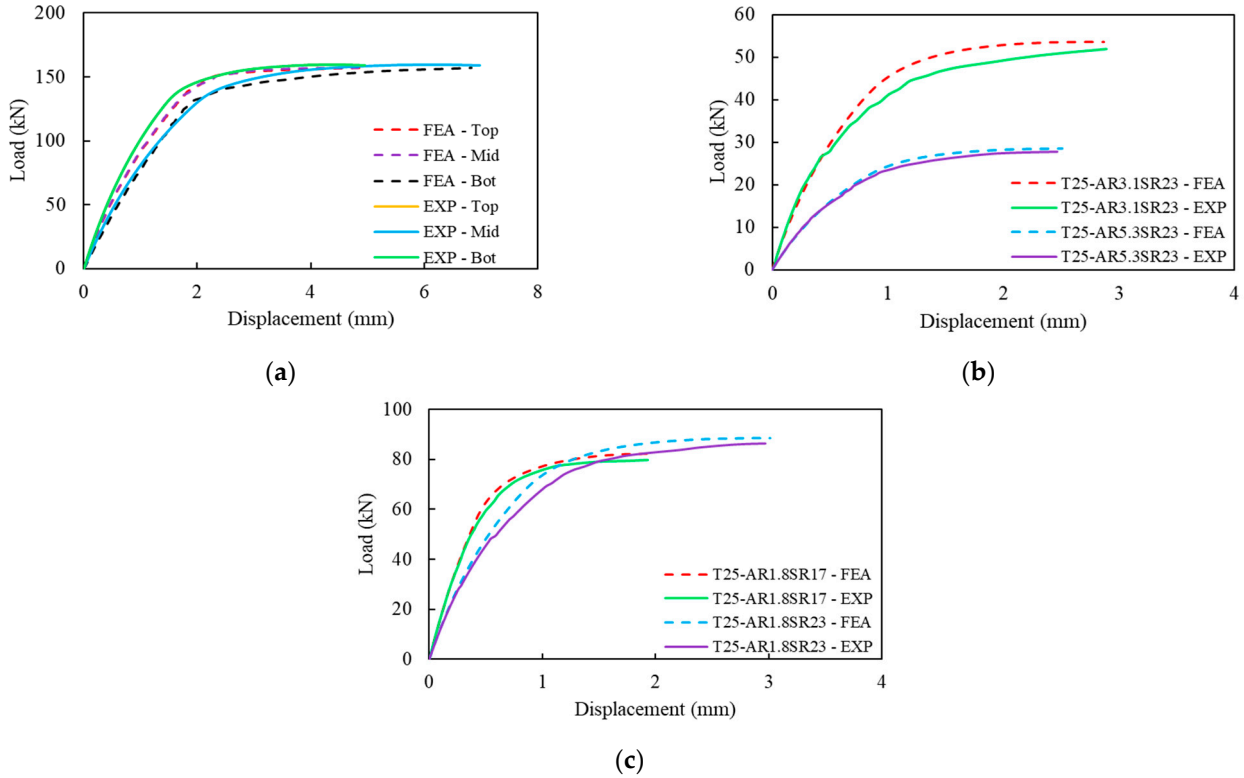

Figure 8. Comparison between FEA and experimental results: (**a**) T60-AR5.3SR23, (**b**) T25-AR3.1SR23 and T25-AR5.3SR23, (**c**) T25-AR1.8SR17 and T25-AR1.8SR23.

4.1.3. Deflection Corresponding to Ultimate Failure Load

The maximum deflections corresponding to ultimate failure load are tabulated in Table 7. The deflections are expressed as a deflection ratio for comparison. The table shows that specimens T60-AR5.3SR23 and T25-AR5.3SR23 have similar deflection ratios due to similar geometry ratios. On the other hand, when the slenderness ratio increases from 17 to 23, the deflection ratio increases from 0.0045 to 0.0053 for T25-AR1.8SR17 and T25-AR1.8SR23, respectively. This is due to the increased flexibility provided by a longer effective length as a result of a higher slenderness ratio. When the aspect ratio of the specimen increases from 1.8 to 3.1 and 5.3, the deflection ratio shows a decreasing trend from 0.0053 to 0.0051 and 0.0044, respectively. This is due to the fact that as the aspect ratio decreases, the cross-sectional area of the concrete wall decreases, lowering the maximum ultimate failure load. Generally, the lateral deflections of OPS-based concrete wall are relatively small and fall within the limits of conventional design provisions.

Table 7. Maximum deflections.

Specimens	Maximum Deflection, Δ (mm)	Specimen Height, H (mm)	Deflection Ratio, Δ/H
T25-AR1.8SR17	1.93	425	0.0045
T25-AR1.8SR23	2.97	565	0.0053
T25-AR3.1SR23	2.89	565	0.0051
T25-AR5.3SR23	2.46	565	0.0044
T60-AR5.3SR23	6.4	1400	0.0046

4.1.4. Ultimate Failure Load

Average failure load and corresponding standard deviation of the test specimens are summarized in Table 8. The failure loads have been expressed as axial strength ratios. This allows for a discernible comparison of ultimate axial capacity of concrete wall specimens

with different cross-sectional areas. The average axial strength ratios of test specimens are in the range of 0.64 to 0.83. Significant reduction is noticed when slenderness ratio increases from 17 (T25-AR1.8SR17) to 23 (T25-AR1.8SR23), with the axial strength ratio decreased from 0.78 to 0.64. This finding showed that geometrical nonlinearity (i.e., slenderness ratio) has great influence on the load-carrying capacity of concrete wall [37]. Failure of slender wall is dominated by buckling mode in which the lateral deflection increases due to vertical loading, thus inducing secondary eccentricity that causes the wall to fail before material failure. Experimental failure loads are then compared to the results determined from ACI 318, AS 3600, and Eurocode 2. It is noticed that the design equations of the standards have safely and conservatively predicted the failure load of lightweight concrete wall. To be specific, the P_{cal}/P_{exp} ratio of the ACI equation varies from 0.38 to 0.58. The underestimation of the ACI equation is mainly due to the assumption made by the ACI equation that loading is applied within the eccentricity of t/6. The experiments in this research were carried out with concentric loading. Therefore, the underestimation made by the ACI equation proves that it is not suitable to determine the ultimate load of concrete wall with other eccentricities. As for the AS 3600 design equation, the P_{cal}/P_{exp} ratio varies from 0.46 to 0.61. The ultimate strength of concrete wall loaded at different values of eccentricity can be determined by the AS 3600 equation. However, this equation still underestimates the ultimate strength of lightweight wall without reduction factor, as shown in this research. The comparisons of experimental and calculated results have highlighted that the AS 3600 equation has the limitation in which the equation is conservative, and no parameter is allowed for lightweight concrete wall. Among the design equations from the three standards, Eurocode 2 gives load estimation with the best accuracy. The P_{cal} $/P_{exp}$ ratio varies from 0.91 to 0.66. However, the Eurocode 2 equation becomes less accurate when the slenderness ratio is increased. Nevertheless, this design equation takes into consideration parameters similar to AS 3600 but appears to show better results accuracy when compared to AS 3600. Unfortunately, similar to the other three standards, Eurocode 2 does not have a parameter to consider the effect of the material property of lightweight concrete.

Table 8. Experimental results.

Specimens	Average Failure Load P_{exp} (kN)	Standard Deviation of Test Results	Average Axial Strength Ratio Pexp/f′cAg	ACI P_{cal} (kN)	AS P_{cal} (kN)	Eurocode 2 P_{cal} (kN)
T25-AR1.8SR17	78	2.25	0.78	40.83	44.6	63.51
T25-AR1.8SR23	85.59	1.8	0.64	39.81	46.42	66.33
T25-AR3.1SR23	51.2	1.31	0.65	23.43	27.31	39.01
T25-AR5.3SR23	27.32	0.6	0.68	10.46	12.52	18.06
T60-AR5.3SR23	155.06	2.25	0.71	60.03	71.07	101.97

Generally, the lightweight concrete wall has a lower axial strength ratio due to its lower elastic modulus, which is required for resisting bending moment arising from eccentricity and slenderness effect. However, the design equations provided by various design standards are still conservative in determining its ultimate capacity. None of the design equations provide a factor to allow for lightweight concrete material property. This has demonstrated that the design equations from the standards need to be improved if they are to more accurately predict the axial strength of concrete wall, regardless of it being manufactured from lightweight or normal-weight concrete.

4.2. Effect of Specimen Size

With respect to walls of similar geometry ratio, both the larger wall (T60-AR5.3SR23) and smaller wall (T25-AR5.3SR23) have shown similar failure modes and cracking patterns. As illustrated in Figure 7a,b, both walls failed by buckling in a single curvature with a horizontal crack developed near mid height. Similar stress distribution has been manifested

in both cases. For the ease of comparison between specimens with different scale, the failure loads are converted into axial strength ratio. As shown in Table 8, the axial strength ratio of T25-AR5.3SR23 is 0.68, while T60-AR5.3SR23 is 0.71. Both specimens have the same slenderness and aspect ratio but different values of thickness. Comparison of specimens with similar geometry ratios shows that specimen T25-AR5.3SR23 and T60-AR5.3SR23 have close axial strength ratios, with differences of 4%. It can be established that concrete walls with a similar geometry ratio possess similar axial strength ratio even if their dimensions are different. Thus, the specimen size effect is negligible.

4.3. FEA Model Validation

In order to validate the constructed model, a comparison is made between the FEA and test results of this study and the published literature [28,43]. The comparison is made in terms of failure characteristics including failure mode, load versus deflection behavior, and ultimate axial load capacity. Figure 7 shows the comparison of experimental and FEA failure modes for concrete wall specimens. In ABAQUS, the maximum principle plastic strain can be used to show the concrete crack pattern. The FEA model has predicted these specimens to fail in buckling failure mode. As shown in Figure 7, it is noted that plastic strains are concentrated at the mid height of these specimens. Specifically, a horizontal crack develops at the mid height of the wall panel. These specimens show uniaxial curvature deformation with maximum deflection at mid height. The cracking pattern and failure mode of lightweight concrete wall have been well predicted by the CDP model in ABAQUS.

The comparison between experimental and FEA load versus deflection curves are shown in Figure 8. It can be observed that the results of the FEA with respect to the ultimate axial capacity and deflections are in good agreement with the experimental results. In general, the FE model has shown a slightly stiffer response at the nonlinear region. This is mainly because idealistic concrete material characteristics are assumed in the modelling process. The comparison demonstrates that the CDP model in ABAQUS gives a good prediction of the nonlinear load-deflection behavior of lightweight concrete wall, as the modelling results are well correlated with experimental values.

Table 9 summarizes the comparisons between FEA results and experimental results for all lightweight wall panels in terms of ultimate axial capacity. FEA and experimental results are expressed as P_{FEA}/P_{exp} ratio for the purpose of comparison. The comparison indicates that the P_{FEA}/P_{exp} ratios ranged from 1.03 to 1.05 for the experimental results of this study. The P_{FEA}/P_{exp} ratios of the benchmarked model [28,43] ranged from 0.9 to 1.12. Overall, P_{FEA}/P_{exp} ratio has mean value of 1.04 and standard deviation of 0.06. The comparison of results shows that the predicted ultimate axial capacity of FEA model is satisfactory, albeit with a slight overestimation. The slight discrepancies of FEA results are mainly due to the idealistic nature of the FEA model, including materials and boundary conditions [63]. The CDP model gives a more accurate prediction of the ultimate axial capacity of lightweight concrete wall compared to the results calculated using design equations of various design standards.

From the comparison between the FEA results and those obtained experimentally with regard to failure mode, load versus deflection behavior, and ultimate axial capacity, it is demonstrated that the CDP model in ABAQUS can accurately predict the structural behavior of axially loaded wall. This also clearly demonstrates the reliability of ABAQUS as a powerful tool for the analysis of concrete wall under axial loading.

Table 9. Comparison of failure loads.

Study	Specimen	P_{exp} (kN)	P_{FEA} (kN)	P_{FEA}/P_{exp} Ratio
Present Study	T25-AR1.8SR17	78	82.31	1.06
	T25-AR1.8SR23	85.59	88.53	1.03
	T25-AR3.1SR23	51.2	53.55	1.05
	T25-AR5.3SR23	27.32	28.55	1.05
	T60-AR5.3SR23	155.06	159.68	1.03
Saheb and Desayi [28]	WSR1	214.18	192.4	0.90
	WSR2	254.1	246.87	0.97
	WSR3	298.92	319.1	1.07
	WSR4	373.65	409.67	1.10
	WSTV4	704.14	787.66	1.12
	WSTV7	463.28	430.94	0.93
	WSTH6	348.74	362.97	1.04
Doh and Fragomeni [43]	OWNS3	426.7	462.25	1.08
	OWNS4	441.5	443.63	1.00
	OWHS2	482.7	504	1.04
	OWHS3	441.5	462.45	1.05
	OWHS4	455.8	495.71	1.09
Mean				1.04
Standard Deviation				0.06

5. FEA Parametric Study

5.1. Effect of Slenderness Ratio

Slenderness ratio is a significant parameter that affects the axial strength ratio of concrete wall. Figure 9 shows the curves of axial strength ratio versus slenderness ratio with different values of eccentricity. In the study, the slenderness ratio is varied from 23 to 50. The slenderness ratio parameter is studied with four different eccentricities (t/600, t/20, t/12, t/6). It is noted that the shape of the curve is sensitive to the change in eccentricity. At the eccentricity of t/600, the decrease in axial strength ratio with an increase in slenderness ratio gives a downward concave curvature shape. When the eccentricity is increased to t/12, the shape of the curve becomes flat and shows a slightly upward concave shape. The concave shape of the curve is more noticeable when the eccentricity is increased to t/6. Initial eccentricity is important in determining the profile of axial strength versus slenderness ratio.

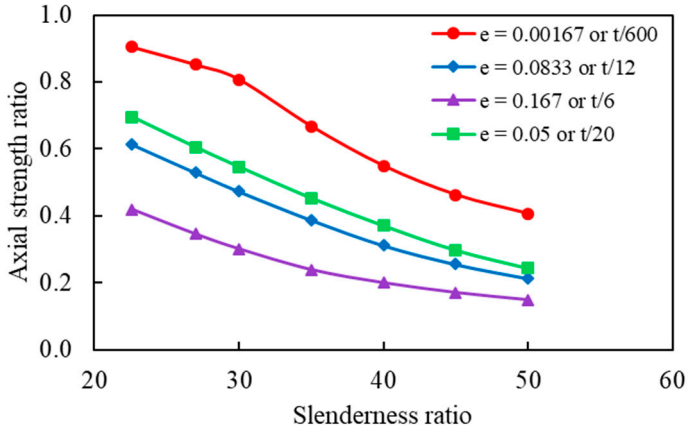

Figure 9. Axial strength ratio versus slenderness ratio with different eccentricities.

It is important to note that the axial strength of the concrete wall decreases nonlinearly with increase of slenderness ratio due to geometrical nonlinearity. At eccentricity of t/600, the axial strength ratio of wall decreases from 0.904 to 0.406 when the slenderness ratio is increased from 23 to 50. Approximately 55% reduction in strength is observed. Likewise,

when eccentricity is increased to t/12 and t/6, the axial strength ratio decreases from 0.614 to 0.213 and from 0.419 to 0.149, respectively, when the slenderness ratio is increased from 23 to 50. At the eccentricities of t/12 and t/6, a reduction of about 65% in strength is observed when the slenderness ratio is increased. It is crucial to note that concrete wall with slenderness ratio greater than 30, and even up to 50, is still able to sustain load. This has further highlighted the limitation of design equations in the standard in which negative strength values result for the slenderness ratios higher than 30. This study also confirms previous findings of Doh and Fragomeni [43].

The concrete wall with a higher slenderness ratio has a longer effective length. It has a higher tendency to buckle, and therefore its lateral deflection increases significantly when loaded. The significant increase in lateral deflection results in an increase in secondary moment, and hence reduces the axial strength ratio. The axial strength ratio decreases nonlinearly with an increase in the slenderness ratio.

5.2. Effect of Eccentricity

Eccentricity exists when the applied load is offset from the centroid of wall, creating bending stress along with axial stress. The eccentricity effect is investigated at values of t/600 to t/20, t/12, and t/6. Figure 9 shows the change in axial strength ratio with slenderness ratio at different eccentricities. As discussed previously, the shape of the axial-strength-to-slenderness ratio curve changes from a downward concave shape to an upward concave shape when the eccentricity is increased. At low eccentricity of t/600, the reduction of axial strength ratio with slenderness ratio is more significant when compared to a higher eccentricity. The slenderness ratios of 30 to 40 show the most remarkable decrease in strength. Strength reduction tapers off in the range from 40 to 50. When the eccentricity is increased to t/20 and subsequently t/12, a smooth reduction of the axial strength ratio with no sharp drop is observed. Similarly, the strength reduction is also observed to taper off in the slenderness ratio range from 40 to 50. At eccentricity of t/6, it is noted that the reduction of axial strength ratio with increase of slenderness ratio is less severe. This can be explained that at higher eccentricity, the primary moment due to eccentricity is relatively large when compared to the secondary moment. At a lower slenderness ratio of 23, the axial strength ratio decreases from 0.904 to 0.694, 0.614, and 0.419 when the eccentricity is increased from t/600 to t/20, t/12, and t/6 respectively. At a high slenderness ratio of 50, when eccentricity is increased from t/600 to t/20, t/12, and t/6, the axial strength ratio decreases from 0.406 to 0.243, 0.213, and 0.149, respectively. The change of axial strength ratio versus slenderness ratio envelope with eccentricity shows a similar trend to that of reinforced concrete column [64]. For concrete wall with one side edge restrained [65], the envelope of axial strength ratio versus slenderness ratio also changes from a downward concave shape to an upward concave shape when the eccentricity is increased.

5.3. Effect of Compressive Strength

Figure 10 shows a comparison of the ultimate axial capacity of concrete wall when the compressive strength is varied from 13.7 to 80 MPa. It is noted that the increase in axial strength ratio is not directly proportional to the increase in concrete compressive strength. For instance, when the slenderness ratio is fixed at 22.6 and at eccentricity of t/20, the ultimate capacity increases by 1.62, 2.32, 2.9, and 3.32 times when the compressive strength is increased from 13.7 MPa to 25, 40, and 80 MPa, respectively. It is noted that the axial strength ratio decreases with an increase in concrete compressive strength. Typically, at a slenderness ratio of 30 and an eccentricity of t/6, the axial strength ratio decreases by 23%, 37%, 50%, and 57%, respectively, when the concrete strength is increased from 13.7 MPa to 25, 40, and 80 MPa. The influences of concrete strength on the axial strength of concrete wall at the eccentricities of t/20, t/12, and t/6 are further illustrated in Figure 10a–c, respectively. These figures show that the envelope decreases as the concrete compressive strength increases. This is in good agreement with Doh and Fragomeni [43] that the ultimate capacity increases nonlinearly with the increase of the compressive strength of

concrete. This is mainly due to the nonlinearity arising from aggregate interlocking at the crack, tensile cracking, and compression crushing of material [66]. Eventually, the ultimate axial strength ratio of the concrete wall decreases with the increase in compressive strength, and its value is also affected by the slenderness ratio and eccentricity value. Current design equations from the standards do not consider the effect of a nonlinear relationship of axial capacity and compressive strength. Linear extrapolation for high-strength concrete can lead to unsafe design.

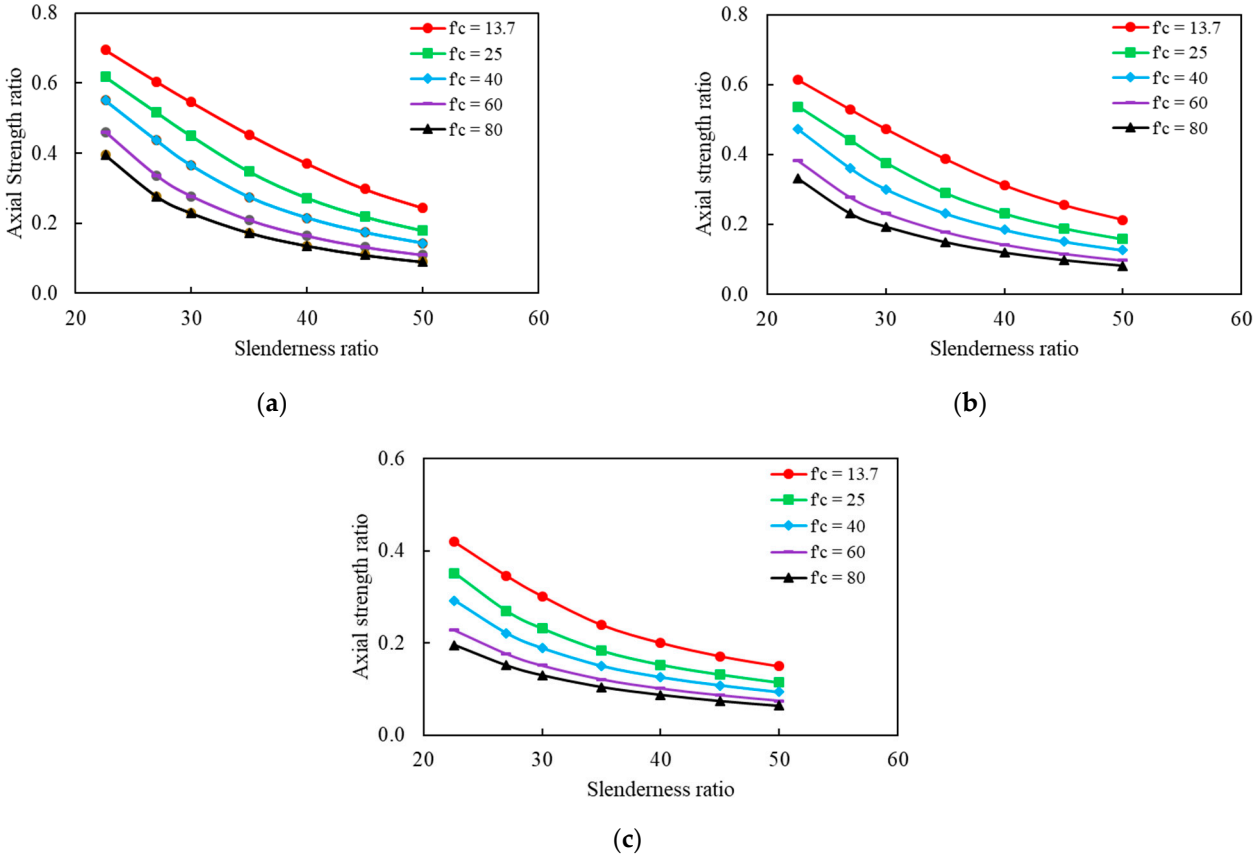

Figure 10. Axial strength ratio versus slenderness ratio with different compressive strength: (**a**) e = 0.05, (**b**) e = 0.0833, (**c**) e = 0.1667.

5.4. Effect of Elastic Modulus

The elastic modulus of concrete is varied in order to study its effect on the axial capacity of concrete wall. The elastic modulus is determined from the density of concrete by using Equation (1). The range of concrete density for this study is from 1600 to 2400 kg/m^3, and the FEA results are illustrated in Figure 11. The range of density studied has been chosen with consideration of the common density of OPS-based lightweight concrete [10] and encompasses lightweight, semi-lightweight, as well as normal-weight concrete. Decrease in elastic modulus with a constant low eccentricity and a low slenderness ratio results in a decrease in both ultimate axial capacity and axial strength ratio. It is noted that the P_{fea}/P_{2400} ratio decreases as the concrete elastic modulus decreases. At eccentricity of t/20 and slenderness ratio 23, by decreasing the elastic modulus from 18,713 to 10186 MPa, the axial strength decreases by 7%. The effect of elastic modulus reduction on axial capacity is more pronounced with increase of slenderness ratio. At eccentricity of t/20 and slenderness ratio of 50, the decrease in elastic modulus has resulted in 39% strength reduction. For higher values of eccentricity and a constant slenderness ratio, the axial capacity of the wall also decreases with a decrease in elastic modulus. For example, at a slenderness ratio of 23, when elastic modulus decreases from 18,713 to 10,186 MPa, the axial capacity decreases by 7%, 8%, and 13% for eccentricities of t/20, t/12, and t/6, respectively.

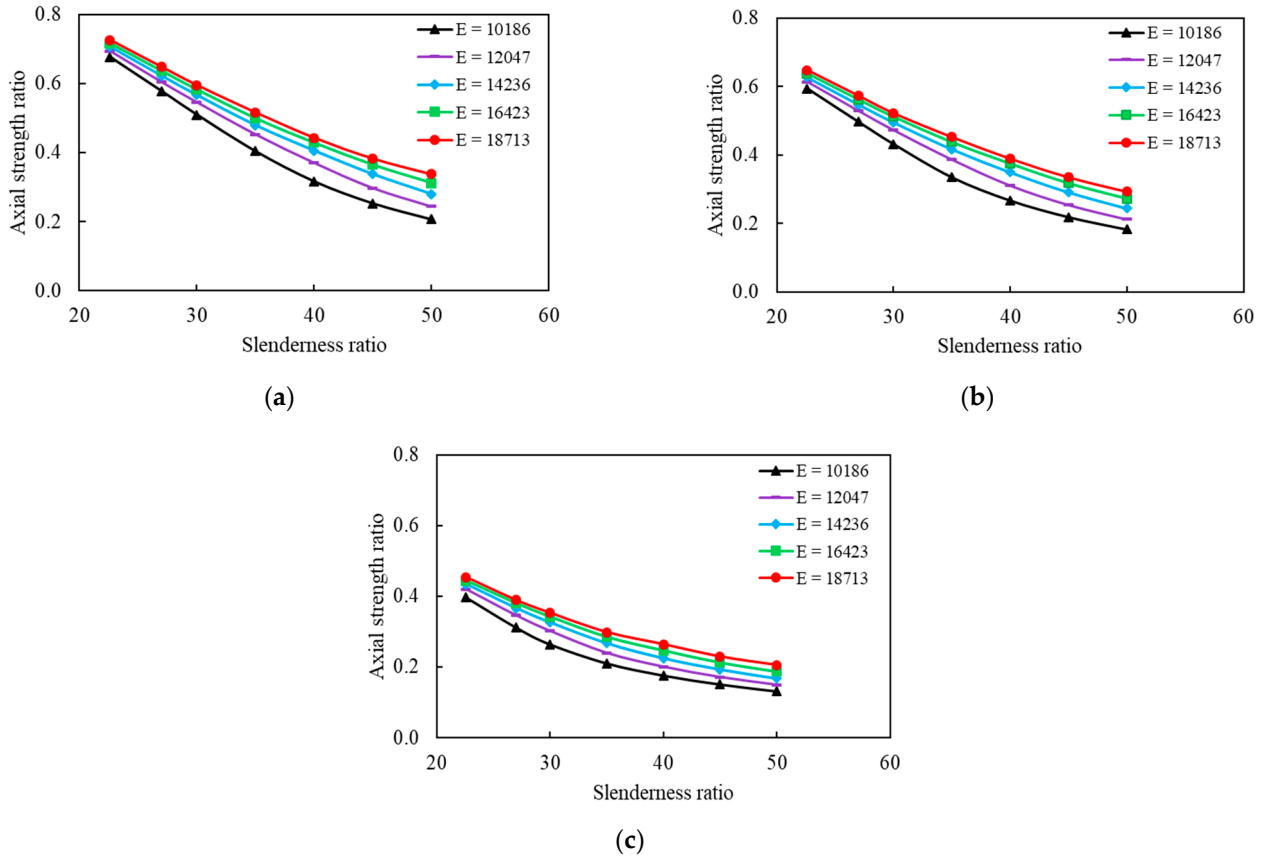

Figure 11. Axial strength ratio versus slenderness ratio with varying elastic modulus: (**a**) e = 0.05, (**b**) e = 0.0833, (**c**) e = 0.1667.

The plots of axial strength ratio versus slenderness ratio with varying elastic modulus at eccentricities of t/20, t/12, and t/6 are illustrated in Figure 11a–c, respectively. It is observed that the curves of axial strength ratio versus slenderness ratio shift downwards when the elastic modulus of concrete decreases at a given compressive strength. As described previously, lightweight concrete exhibits more ductile stress-strain behavior under compression when compared to normal-weight concrete at a given compressive strength [44,45]. This is due to the reduced elastic modulus resulting from the use of lightweight aggregates in concrete. The ultimate load capacity of the concrete wall under axial loading depends not only on the axial stiffness of the wall but also on the flexural stiffness of the wall section. The flexural stiffness of the concrete wall is used to resist the moment induced by both eccentric loading and the second-order effect resulting from lateral deflection. The reduced elastic modulus of lightweight concrete results in reduced flexural stiffness, which is required for resisting the bending moment produced by the effects of eccentricity and slenderness, and hence reduced axial capacity [64]. However, all the current simplified design equations from design standards and published literature do not consider the effect of elastic modulus. The effect of elastic modulus must be considered in the design equation in order to safely predict the axial capacity of lightweight concrete wall.

6. Proposed Design Equation

Based on experimental tests and numerical simulations, it is noted with better insight that the axial capacity of concrete wall is affected by not only its geometry nonlinearity but also its material properties. As mentioned previously, there are limitations in the current design equations from the standards. Current design equations from AS 3600 and Eurocode 2 consider only the effect of slenderness ratio and eccentricity. The design equation of ACI

318 considers only the slenderness ratio. In any case, the equations are only applicable for slenderness ratios of up to 30. In addition, these equations are not suitable for designing lightweight concrete walls. The results obtained from the FEA parametric studies have shown that the axial strength ratio decreases as the elastic modulus of concrete decreases due to the use of lightweight aggregate. Furthermore, the axial strength of concrete wall increases nonlinearly with the increase of compressive strength. Notably, the existing design equations do not take into account the effects of both the compressive strength and the elastic modulus. As such, the design equations need to be enhanced to determine the axial capacity of the concrete wall with better accuracy. In this section, a new semi-empirical equation is proposed to take into consideration the material compressive strength and elastic modulus.

The proposed design equation is derived from equivalent rectangular concrete stress block and the regression analysis. The following are the assumptions made in the derivation of the equation:

1. The wall must contain minimum reinforcement in both vertical and horizontal directions as specified by the AS3600 standard;
2. The loads are within the stress block of the section;
3. The wall behaves as one-way wall under axial loading.

Figure 12 shows the stress block of the concrete wall cross-section. From the equivalent rectangular stress block, the compression force can be determined as Equation (17).

$$P_{us} = \alpha_2 \gamma f'_c A_g \quad (17)$$

where

$$\alpha_2 = 0.85 - 0.0015 f'_c,\ \alpha_2 \geq 0.67$$

$$\gamma = 0.97 - 0.0025 f'_c,\ \gamma \geq 0.67$$

$$f'_c = \text{Compressive strength of concrete}$$

$$A_g = \text{Cross sectional area of wall}$$

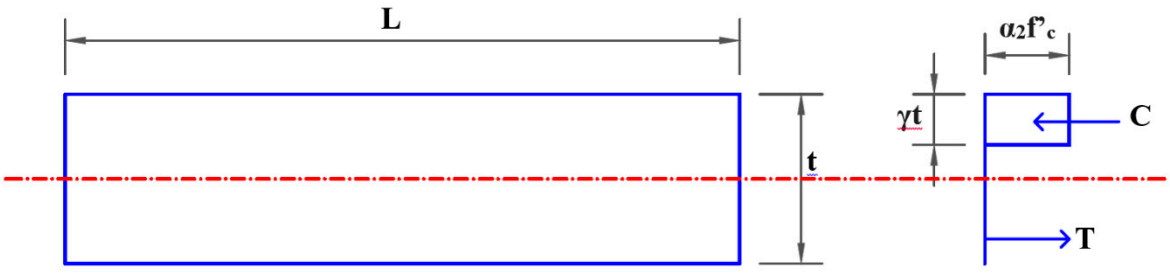

Figure 12. Concrete stress block.

Eccentricity and slenderness ratio parameters are introduced in Equation (17) using regression analyses of the FEA results. Details of regression analyses are shown in Figure 13a,c for the eccentricity ratio at t/20, t/12, and t/6, respectively. Similar approaches to Saheb and Desayi [28] and Ganesan, Indira and Santhakumar [36] are used in the derivation of the equation. Notwithstanding, instead of using quadratic regression for the effect of slenderness ratio, the exponential function has shown a better fitting and is therefore adopted in this equation derivation. The regression equations in Figure 13a,c show the same argument value in exponential function with different constant values. Therefore, another regression analysis is performed to introduce the constant value for different eccentricities, as shown in Figure 13d. Equation (17) then becomes Equation (18).

$$P_{us1} = \alpha_2 \gamma f'_c A_g \exp(-0.038\lambda) e_L \quad (18)$$

where

$$\exp(-0.038\lambda)e_L \leq 1 \quad (19)$$

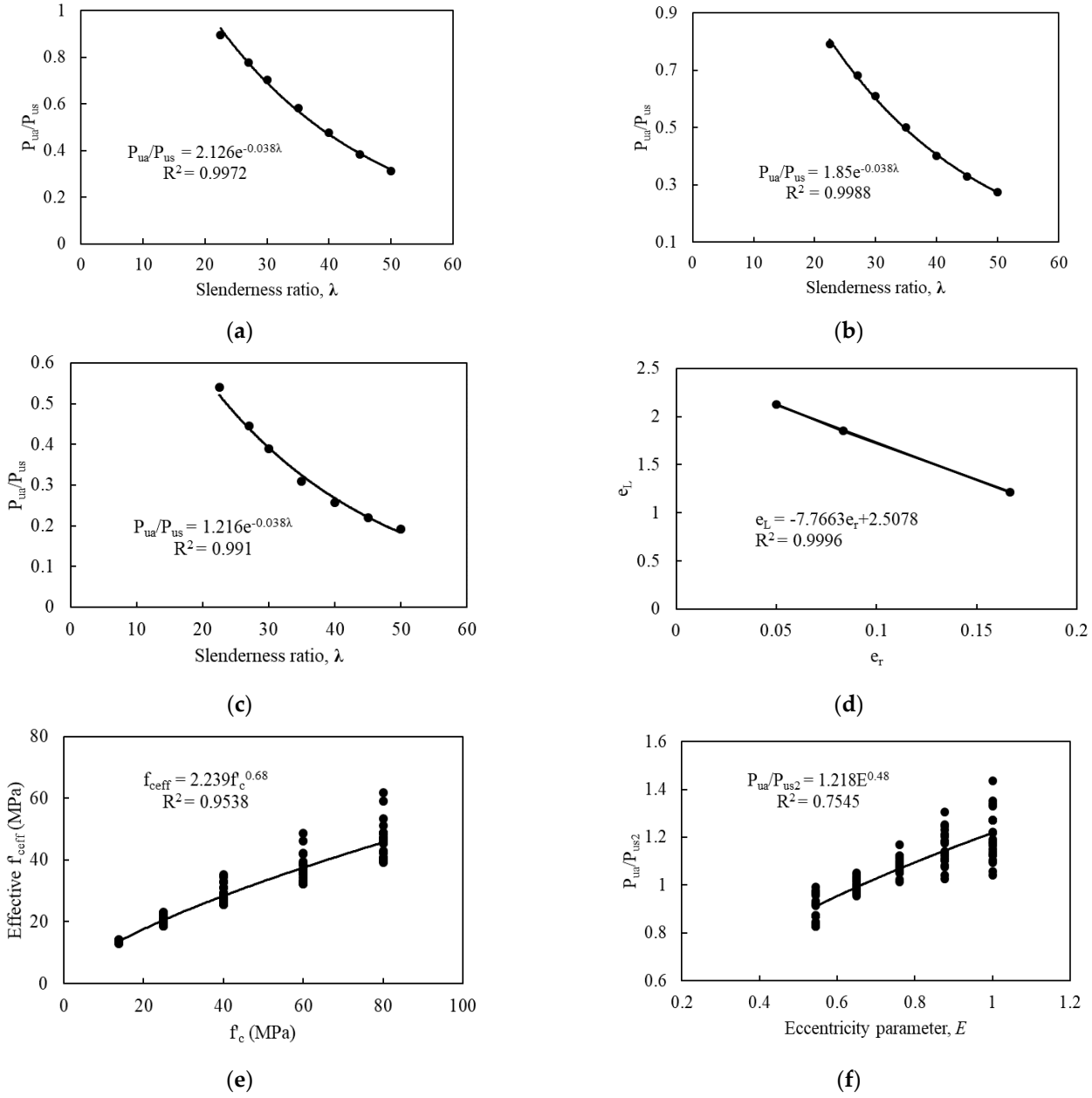

Figure 13. Regression analysis for (**a**) λ at e = t/20, (**b**) λ at e = t/12, (**c**) λ at e = t/6, (**d**) parameter e, (**e**) f′c, (**f**) parameter E.

The eccentricity parameter is determined from

$$e_L = 7.77e_r + 2.51 \quad (20)$$

where

λ = Slenderness ratio

e_L = Eccentricity parameter

e_r = Eccentricity ratio of applied load to total wall thickness

Equation (18) is rearranged with f′c expressed in terms of other variables, and this effective f′c value is then plotted against the actual f′c, as illustrated in Figure 13e. From the

regression analysis, the compressive strength of concrete is represented by a power function of the f'_c variable raised to a fixed power of 0.68. This is to account for the nonlinear increase in axial capacity as concrete strength increases. Equation (18) is subsequently transformed into Equation (21).

$$P_{us2} = 2.24\alpha_2\gamma f'^{0.68}_c A_g \exp(-0.038\lambda)e_L \quad (21)$$

Another factor, the E variable, has been introduced to account for the effect of different values of concrete elastic modulus on its axial capacity. In order to introduce the factor for elastic modulus, the P_{ua}/P_{us2} values derived from the FEA results and Equation (21) are plotted against E, as shown in Figure 13f. The E variable is also represented by a power function raised to a fixed power of 0.48. This factor is calibrated from the results of the FE model by using regression analysis. The final design equation is depicted as Equation (22).

$$P_u = 2.73\alpha_2\gamma f'^{0.68}_c A_g \exp(-0.038\lambda)e_L E^{0.48} \quad (22)$$

The elastic modulus parameter, E can be determined from Equation (23).

$$E = \frac{E_c}{E_{2400}} \quad (23)$$

where

E = Elastic modulus parameter

E_c = Elastic modulus of concrete

E_{2400} = Reference elastic modulus of concrete when $\rho = 2400\ kg/m^3$

From Equation (22), the axial strength of concrete wall varies with eccentricity (e_L) and slenderness ratio (λ). The nonlinear increase in axial strength with the compressive strength ($f'^{0.68}_c$) is reflected in the equation. In addition, the axial strength reduction due to the use of lightweight aggregate is allowed for by means of the elastic modulus parameter (E).

Equation Validation

In order to verify the validity of the proposed equation, comparisons are made between the calculated results from the proposed equation and the experimental results. Table 10 shows the calculated results of the proposed and existing equations. The geometric and material properties from the published literature used for benchmarking are provided in Table A1. Using the proposed equation, the P_{cal}/P_{exp} ratio of this study ranged from 0.88 to 1, while the P_{cal}/P_{exp} ratio from the published literature ranged from 0.8 to 1.14. The calculated results from the proposed equation are slightly conservative in predicting the axial strength of the lightweight concrete wall with all P_{cal}/P_{exp} ratios of less than 1. As shown in Table 10, none of the existing equations provide a good axial strength prediction for lightweight concrete wall. The proposed design equation gives better prediction of the axial capacity of lightweight concrete wall compared to the existing equations. It can be seen that the proposed equation gives an improved estimation of the axial strength of normal-weight concrete wall compared with the existing equations. For highstrength concrete wall, the axial strength prediction using Equation (22) shows slight overestimation for specimens OWHS3 and OWHS4 [43], with P_{cal}/P_{exp} ratios of 1.14 and 1.11, respectively. The compressive strengths of these specimens are 63 and 75.9 MPa, respectively, while the slenderness ratios are 35 and 40, respectively. As for the high-strength concrete walls of Fragomeni and Mendis [35], the calculated results from Equation (22) are slightly conservative with P_{cal}/P_{exp} ratios of 0.92, 0.96, and 0.89 for specimens 2b, 5b, and 6b, respectively. The compressive strengths of these specimens are 65.4, 59.7, and 67.4 MPa, respectively, whereas the slenderness ratios are 15, 20, and 25, respectively. These comparisons manifest that the proposed equation can give a good prediction of the ultimate capacity of the normal-weight high-strength slender wall. The

comparisons demonstrate that the predicted results obtained have shown a good agreement with both the present and published experimental results.

Table 10. Comparison between experimental and calculated results.

	Specimen	ACI	AS	EC 2	Equation (22)
		P_{cal}/P_{exp}	P_{cal}/P_{exp}	P_{cal}/P_{exp}	P_{cal}/P_{exp}
Present study	T25-AR1.8SR17	0.52	0.56	0.80	0.88
	T25-AR1.8SR23	0.46	0.54	0.77	1.00
	T25-AR3.1SR23	0.45	0.53	0.75	0.97
	T25-AR5.3SR23	0.38	0.46	0.66	0.94
	T60-AR5.3SR23	0.39	0.46	0.66	0.97
Saheb and Desayi [28]	WAR1	0.78	0.68	0.75	1.06
	WAR2	0.80	0.70	0.77	1.08
	WAR3	0.85	0.74	0.81	1.14
	WSR1	0.62	0.54	0.64	0.88
	WSR2	0.65	0.56	0.62	0.88
	WSR3	0.66	0.57	0.52	0.89
	WSTV2	0.80	0.70	0.76	1.03
	WSTV3	0.73	0.64	0.70	0.94
	WSTH2	0.78	0.67	0.74	1.01
Fragomeni and Mendis [35]	2a	0.92	0.79	0.67	0.87
	2b	1.25	1.07	0.91	0.92
	5a	0.76	0.64	0.42	1.02
	5b	0.95	0.80	0.52	0.96
	6b	1.30	1.13	1.13	0.89
Doh and Fragomeni [43]	OWNS3	N.A.	N.A.	N.A.	1.10
	OWNS4	N.A.	N.A.	N.A.	0.99
	OWHS3	N.A.	N.A.	N.A.	1.14
	OWHS4	N.A.	N.A.	N.A.	1.11
Ganesan, Indira and Santhakumar [36]	OPCAR1	0.81	0.70	0.70	0.81
	GPCSR1	0.78	0.68	0.75	0.80
	GPCAR1	0.86	0.74	0.75	0.87
Mean		0.36	0.31	0.34	0.97
Standard Deviation		1.05	0.97	0.96	0.10

The comparisons have manifested that the proposed equation yield a more accurate prediction of the axial strength of concrete wall. Hence, it can be regarded as an improved equation for the design of axially loaded concrete wall.

7. Conclusions

Though the compression behavior of OPS-aggregate-based concrete has been widely studied at the material level, there is limited research on its buckling behavior under axial loading as a structural component. This research studied the buckling behavior of LWSCC wall incorporated with OPS. With the investigation through experiment and numerical studies, the following conclusions can be drawn:

1. It is found that the axial load-deflection behavior of OPS-based LWSCC wall shows linear responses in the initial loading region, which are followed by nonlinear response up to ultimate failure load. The ultimate axial strength of lightweight wall decreases with an increase in the slenderness ratio.
2. From the comparisons, it can be seen that the existing design equations from the standards provide conservative estimation with P_{cal} /P_{exp} ratios ranging from 0.36 to 0.91 and are not suitable for use in lightweight concrete wall. None of them takes into consideration the material properties of lightweight concrete.
3. From the results of parametric study on the effects of slenderness ratio, it has been demonstrated that concrete wall is still capable of sustaining loading with a slenderness ratio more than 30, and the axial strength ratio decreases nonlinearly with the increase of slenderness ratio.
4. Parametric study shows that the ultimate axial capacity increases nonlinearly with the increase of the compressive strength of concrete. Typically, the axial strength ratio can be decreased nonlinearly by 57% when compressive strength increases from 13.7 MPa to 80 MPa at constant eccentricity of t/6.
5. From parametric study, the analysis has identified the elastic modulus as one of the key parameters determining the ultimate axial strength of concrete wall. Decrease in

elastic modulus of concrete results in a reduced ultimate axial capacity of the wall and vice versa. Elastic modulus of concrete is the key parameter affecting the ultimate axial strength of lightweight concrete wall.

6. A design equation based on the equivalent rectangular stress block concept and incorporated with statistical factors has been proposed, which takes into account the effects of the elastic modulus, slenderness ratio, eccentricity, and nonlinear compressive strength of concrete. The equation has been benchmarked against published data and found to be effective and versatile. With the consideration of concrete elastic modulus and relevant parameters, the proposed design equation is thought to be a more reliable and effective design aid for industrial application. The proposed design equation can be the basis for further development of the equation, taking into account more parameters such as wall openings and side restraints (two-way wall).
7. Hence, considering its lightweight characteristics and self-compacting property, OPS-based LWSCC can be introduced as a sustainable solution for the construction industry to promote not only automation but also environmental conservation. The proposed design equation can serve as a practical design tool to provide insight into the strength of lightweight concrete wall used as an axial component for a sustainable building structure.

Author Contributions: Conceptualization, M.E.R. and H.H.L.; methodology, M.E.R., T.Z.H.T. and H.H.L.; software, T.Z.H.T.; validation, T.Z.H.T. and M.E.R.; formal analysis, H.H.L.; investigation, T.Z.H.T.; resources, M.E.R.; data curation, T.Z.H.T.; writing—original draft preparation, T.Z.H.T.; writing—review and editing, M.E.R., B.N. and K.P.; visualization, T.Z.H.T.; supervision, M.E.R. and H.H.L.; project administration, H.H.L.; funding acquisition, M.E.R. All authors have read and agreed to the published version of the manuscript.

Funding: This research was funded by Curtin Malaysia Research Institute (CMRI) grant number 6020 and the APC was funded by University of Northumbria.

Institutional Review Board Statement: Not applicable.

Informed Consent Statement: Not applicable.

Data Availability Statement: All data generated or appeared in this study are available upon request from the corresponding author.

Acknowledgments: The authors would like to acknowledge full research funding provided by Curtin Malaysia Research Institute (CMRI 6020) and laboratory support provided by Curtin University Malaysia.

Conflicts of Interest: The authors declare no conflict of interest.

Appendix A Specimen Details

The geometric and material properties from the published literature used for benchmarking are summarized in Table A1.

Table A1. Details of published test results.

References	Specimen	H × L × t (mm)	f′c (MPa)	Steel Ratio	fsy (MPa)	Failure Load (kN)
Saheb and Desayi [28]	WAR1	600 × 900 × 50	17.864	0.00173	297	484.27
	WAR2	600 × 600 × 50	17.86	0.00	297	315.8
	WAR3	600 × 400 × 50	17.86	0.00	297	198.29
	WSR1	450 × 300 × 50	17.34	0.00	297	214.18
	WSR2	600 × 400 × 50	17.34	0.00	297	254.1
	WSR3	900 × 600 × 50	17.34	0.00	297	298.92
	WSTV2	600 × 900 × 50	20.14	0.00	286	535.07
	WSTV3	600 × 900 × 50	20.14	0.01	581	583.52
	WSTH2	600 × 900 × 50	19.6	0.00173	297	538.01
Fragomeni and Mendis [35]	2a	1000 × 300 × 50	42.4	0.0025	450	231.8
	2b	1000 × 300 × 50	65.4	0.0025	450	263.5
	5a	1000 × 500 × 40	35.7	0.0025	450	201.2
	5b	1000 × 500 × 40	59.7	0.0025	450	269.2
	6b	600 × 200 × 40	67.4	0.0031	450	178
Doh and Fragomeni [43]	OWNS3	1400 × 1400 × 40	52	0.0031	610	426.7
	OWNS4	1600 × 1600 × 40	51	0.0031	610	441.5
	OWHS3	1400 × 1400 × 40	63	0.0031	610	441.5
	OWHS4	1600 × 1600 × 40	75.9	0.0031	610	455.8
Ganesan, Indira and Santhakumar [36]	OPCAR1	600 × 320 × 40	33.832	0.0088	415	230.53
	GPCSR1	480 × 320 × 40	33.072	0.0088	415	256.18
	GPCAR1	600 × 320 × 40	33.072	0.0088	415	211.89

References

1. Mohammed, S.I.; Najim, K.B. Mechanical Strength, Flexural Behavior and Fracture Energy of Recycled Concrete Aggregate Self-Compacting Concrete. *Structures.* **2020**, *23*, 34–43. [CrossRef]
2. Mo, K.H.; Thomas, B.S.; Yap, S.P.; Abutaha, F.; Tan, C.G. Viability of agricultural wastes as substitute of natural aggregate in concrete: A review on the durability-related properties. *J. Clean. Prod.* **2020**, *275*, 123062. [CrossRef]
3. Ting, T.; Rahman, M.; Lau, H.; Ting, M. Recent development and perspective of lightweight aggregates based self-compacting concrete. *Constr. Build. Mater.* **2019**, *201*, 763–777. [CrossRef]
4. Revilla-Cuesta, V.; Skaf, M.; Faleschini, F.; Manso, J.M.; Ortega-López, V. Self-compacting concrete manufactured with recycled concrete aggregate: An overview. *J. Clean. Prod.* **2020**, *262*, 121362. [CrossRef]
5. Manzi, S.; Mazzotti, C.; Bignozzi, M.C. Self-compacting concrete with recycled concrete aggregate: Study of the long-term properties. *Constr. Build. Mater.* **2017**, *157*, 582–590. [CrossRef]
6. Aslam, M.; Shafigh, P.; Jumaat, M.Z. Oil-palm by-products as lightweight aggregate in concrete mixture: A review. *J. Clean. Prod.* **2016**, *126*, 56–73. [CrossRef]
7. Shafigh, P.; Jumaat, M.Z.; Mahmud, H. Mix design and mechanical properties of oil palm shell lightweight aggregate concrete: A review. *Int. J. Phys. Sci.* **2010**, *5*, 2127–2134.
8. Zawawi, M.N.A.A.; Muthusamy, K.; Majeed, A.P.A.; Musa, R.M.; Budiea, A.M.A. Mechanical properties of oil palm waste lightweight aggregate concrete with fly ash as fine aggregate replacement. *J. Build. Eng.* **2020**, *27*, 100924. [CrossRef]
9. Hamada, H.M.; Thomas, B.S.; Tayeh, B.; Yahaya, F.M.; Muthusamy, K.; Yang, J. Use of oil palm shell as an aggregate in cement concrete: A review. *Constr. Build. Mater.* **2020**, *265*, 120357. [CrossRef]
10. Alengaram, U.J.; Al Muhit, B.A.; bin Jumaat, M.Z. Utilization of oil palm kernel shell as lightweight aggregate in concrete—A review. *Constr. Build. Mater.* **2013**, *38*, 161–172. [CrossRef]
11. Nagaratnam, B.H.; Rahman, M.E.; Mirasa, A.K.; Mannan, M.A.; Lame, S.O. Workability and heat of hydration of self-compacting concrete incorporating agro-industrial waste. *J. Clean. Prod.* **2016**, *112*, 882–894. [CrossRef]
12. Okpala, D. Palm kernel shell as a lightweight aggregate in concrete. *Build. Environ.* **1990**, *25*, 291–296. [CrossRef]
13. Okafor, F.O. Palm kernel shell as a lightweight aggregate for concrete. *Cem. Concr. Res.* **1988**, *18*, 901–910. [CrossRef]
14. Mannan, M.; Alexander, J.; Ganapathy, C.; Teo, D. Quality improvement of oil palm shell (OPS) as coarse aggregate in lightweight concrete. *Build. Environ.* **2006**, *41*, 1239–1242. [CrossRef]
15. Chen, M.; Li, Z.-H.; Wu, J.-F.; Wang, J.-H. Shear behaviour and diagonal crack checking of shale ceramsite lightweight aggregate concrete beams with high-strength steel bars. *Constr. Build. Mater.* **2020**, *249*, 118730. [CrossRef]
16. Teo, D.; Mannan, M.A.; Kurian, V.; Ganapathy, C. Lightweight concrete made from oil palm shell (OPS): Structural bond and durability properties. *Build. Environ.* **2007**, *42*, 2614–2621. [CrossRef]
17. Shafigh, P.; Jumaat, M.Z.; Mahmud, H. Oil palm shell as a lightweight aggregate for production high strength lightweight concrete. *Constr. Build. Mater.* **2011**, *25*, 1848–1853. [CrossRef]
18. Farahani, J.N.; Shafigh, P.; Alsubari, B.; Shahnazar, S.; Mahmud, H.B. Engineering properties of lightweight aggregate concrete containing binary and ternary blended cement. *J. Clean. Prod.* **2017**, *149*, 976–988. [CrossRef]
19. Mannan, M.A.; Ganapathy, C. Engineering properties of concrete with oil palm shell as coarse aggregate. *Constr. Build. Mater.* **2002**, *16*, 29–34. [CrossRef]
20. Alengaram, U.J.; Jumaat, M.Z.; Mahmud, H. Ductility behaviour of reinforced palm kernel shell concrete beams. *Eur. J. Sci. Res.* **2008**, *23*, 406–420.

21. Fanijo, E.; Babafemi, A.J.; Arowojolu, O. Performance of laterized concrete made with palm kernel shell as replacement for coarse aggregate. *Constr. Build. Mater.* **2020**, *250*, 118829. [CrossRef]
22. Alsalami, Z.H.A.; Harith, I.K.; Dhahir, M.K. Utilization of dates palm kernel in high performance concrete. *J. Build. Eng.* **2018**, *20*, 166–172. [CrossRef]
23. Aslam, M.; Shafigh, P.; Nomeli, M.A.; Jumaat, M.Z. Manufacturing of high-strength lightweight aggregate concrete using blended coarse lightweight aggregates. *J. Build. Eng.* **2017**, *13*, 53–62. [CrossRef]
24. Shafigh, P.; Jumaat, M.Z.; Mahmud, H.B.; Hamid, N.A.A. Lightweight concrete made from crushed oil palm shell: Tensile strength and effect of initial curing on compressive strength. *Constr. Build. Mater.* **2012**, *27*, 252–258. [CrossRef]
25. Shafigh, P.; Nomeli, M.A.; Alengaram, U.J.; Mahmud, H.B.; Jumaat, M.Z. Engineering properties of lightweight aggregate concrete containing limestone powder and high volume fly ash. *J. Clean. Prod.* **2016**, *135*, 148–157. [CrossRef]
26. Doh, J.-H.; Fragomeni, S.; Kim, J.-W. Brief review of studies on concrete wall panels in one and two way action. *Int. J. Ocean. Eng. Technol. Spec. Sel. Pap.* **2001**, *4*, 38–43.
27. Delatte, N. *Failure, Distress and Repair of Concrete Structures*; Elsevier: Amsterdam, The Netherlands, 2009.
28. Saheb, S.M.; Desayi, P. Ultimate strength of RC wall panels in one-way in-plane action. *J. Struct. Eng.* **1989**, *115*, 2617–2630. [CrossRef]
29. Saheb, S.M.; Desayi, P. Ultimate strength of RC wall panels in two-way in-plane action. *J. Struct. Eng.* **1990**, *116*, 1384–1402. [CrossRef]
30. Ganesan, N.; Indira, P.; Prasad, S.R. Strength and behavior of SFRSCC and SFRC wall panels under one-way in-plane action. In *High Performance Fiber Reinforced Cement Composites 6*; Springer: Berlin/Heidelberg, Germany, 2012; pp. 279–286.
31. ACI Committee 318. *Building Code Requirements for Structural Concrete (ACI 318-05) and Commentary (ACI 318R-05)*; American Concrete Institute: Farmington Hills, MI, USA, 2005.
32. *AS 3600-2018: Concrete Structures*; Standards Australia Limited: Sydney, Australia, 2018.
33. Institution, B.S. *Eurocode 2: Design of Concrete Structures: Part 1-1: General Rules and Rules for Buildings*; British Standards Institution: London, UK, 2004.
34. Robinson, G.P.; Palmeri, A.; Austin, S.A. Design methodologies for one way spanning eccentrically loaded minimally or centrally reinforced pre-cast RC panels. *Eng. Struct.* **2013**, *56*, 1945–1956. [CrossRef]
35. Fragomeni, S.; Mendis, P. Improved axial load formulae for normal and high strength reinforced concrete walls. *Aust. Civ. Eng. Trans.* **1996**, *38*, 71.
36. Ganesan, N.; Indira, P.; Santhakumar, A. Prediction of ultimate strength of reinforced geopolymer concrete wall panels in one-way action. *Constr. Build. Mater.* **2013**, *48*, 91–97. [CrossRef]
37. Huang, Y.; Hamed, E.; Chang, Z.-T.; Foster, S.J. Theoretical and experimental investigation of failure behavior of one-way high-strength concrete wall panels. *J. Struct. Eng.* **2014**, *141*, 04014143. [CrossRef]
38. Huang, Y.; Hamed, E. Buckling of one-way high-strength concrete panels: Creep and shrinkage effects. *J. Eng. Mech.* **2013**, *139*, 1856–1867. [CrossRef]
39. Oberlender, G.D. *Strength Investigation of Precast Reinforced Concrete Load-Bearing Wall Panels*; The University of Texas at Arlington: Arlington, TX, USA, 1975.
40. Seddon, A. *Concrete Walls in Compression under Short-Term Axial and Eccentric Loads*; IABSE (International Association for Bridge and Structural Engineering): Zürich, Switzerland, 1956.
41. Pillai, S.U.; Parthasarathy, C. Ultimate strength and design of concrete walls. *Build. Environ.* **1977**, *12*, 25–29. [CrossRef]
42. Zielinski, Z.; Troitski, M.; El-Chakieh, E. Bearing capacity tests on precast concrete thin-wall ribbed panels. *PCI J.* **1983**, *28*, 88–103. [CrossRef]
43. Doh, J.-H.; Fragomeni, S. Evaluation of experimental work on concrete walls in one and two-way action. *Aust. J. Struct. Eng.* **2005**, *6*, 37–52. [CrossRef]
44. Lim, J.C.; Ozbakkaloglu, T. Stress–strain model for normal-and light-weight concretes under uniaxial and triaxial compression. *Constr. Build. Mater.* **2014**, *71*, 492–509. [CrossRef]
45. Cui, H.; Lo, T.Y.; Memon, S.A.; Xing, F.; Shi, X. Analytical model for compressive strength, elastic modulus and peak strain of structural lightweight aggregate concrete. *Constr. Build. Mater.* **2012**, *36*, 1036–1043. [CrossRef]
46. Abdurra'uf, M.G.; Jaganathan, J.; Anwar, M.; Leung, H. Experimental studies and theoretical models for concrete columns confined with FRP composites: A review. *World J. Eng.* **2019**, *16*, 509–525.
47. Hegger, J.; Dreßen, T.; Will, N. Zur Tragfähigkeit unbewehrter Betonwände. *Beton-Und Stahlbetonbau* **2007**, *102*, 280–288. [CrossRef]
48. Hegger, J.; Dressen, T.; Will, N. Load-bearing capacity of plain concrete walls. *Mag. Concr. Res.* **2009**, *61*, 173–182. [CrossRef]
49. Leabu, V.F. Problems and Performance of Precast Concrete Wall Panels. *J. Proc.* **1959**, *56*, 287–298.
50. Kripanarayanan, K. Interesting Aspects of the Empirical Wall Design Equation. *J. Proc.* **1977**, *74*, 204–207.
51. Mohamad, N.; Goh, W.I.; Abdullah, R.; Samad, A.A.A.; Mendis, P.; Sofi, M. Structural performance of FCS wall subjected to axial load. *Constr. Build. Mater.* **2017**, *134*, 185–198. [CrossRef]
52. *ASTM C150/C150M-12: Standard Specification for Portland Cement*; ASTM International: West Conshohocken, PA, USA, 2012.
53. Astm, C. *Standard Specification for Fly Ash and Raw or Calcined Natural Pozzolan for Use as a Mineral Admixture in Portland Cement Concrete*; ASTM International: West Conshohocken, PA, USA, 2003; p. 618.

54. Ting, T.Z.H.; Rahman, M.E.; Lau, H.H. Sustainable lightweight self-compacting concrete using oil palm shell and fly ash. *Constr. Build. Mater.* **2020**, *264*, 120590. [CrossRef]
55. *ASTM C39/C39M-18, Standard Test Method for Compressive Strength of Cylindrical Concrete Specimens*; ASTM International: West Conshohocken, PA, USA, 2018; Available online: www.astm.org (accessed on 1 November 2021).
56. *Standard Test Method for Splitting Tensile Strength of Cylindrical Concrete Specimens*; ASTM International: West Conshohocken, PA, USA, 2011.
57. Yang, K.-H.; Mun, J.-H.; Cho, M.-S.; Kang, T.H.-K. Stress-Strain Model for Various Unconfined Concretes in Compression. *ACI Struct. J.* **2014**, *111*, 819. [CrossRef]
58. Systemes, D. *Abaqus Theory Guide*; Version 6.14; Simulia Corporation: Johnston, RI, USA, 2014.
59. Wahalathantri, B.L.; Thambiratnam, D.; Chan, T.; Fawzia, S. A material model for flexural crack simulation in reinforced concrete elements using ABAQUS. In Proceedings of the First International Conference on Engineering, Designing and Developing the Built Environment for Sustainable Wellbeing, Brisbane, Australia, 27–29 April 2011.
60. Hillerborg, A.; Modéer, M.; Petersson, P.-E. Analysis of crack formation and crack growth in concrete by means of fracture mechanics and finite elements. *Cem. Concr. Res.* **1976**, *6*, 773–781. [CrossRef]
61. Nayal, R.; Rasheed, H.A. Tension stiffening model for concrete beams reinforced with steel and FRP bars. *J. Mater. Civ. Eng.* **2006**, *18*, 831–841. [CrossRef]
62. Hui Fan, Y.; Pan Liu, P.; Shen, B.; Ma, K.; Wu, B.; Zheng, T.; Yang, F. Shear-bearing capacity analysis under static force for shear key of the reinforced concrete open-web sandwich slab applied to long-span structure. *Int. J. Struct. Integr.* **2020**, *2*, 195–213. [CrossRef]
63. Ho, N.M.; Doh, J.H. Experimental and numerical investigations of axially loaded RC walls restrained on three sides. *Struct. Des. Tall Spec. Build.* **2018**, *27*, e1459. [CrossRef]
64. Warner, R.F.; Rangan, B.; Hall, A.; Faulkes, K. *Concrete Structures*; Pearson Education Australia: Melbourne, Australia, 1998.
65. Ho, N.M.; Doh, J.H. Prediction of ultimate strength of concrete walls restrained on three sides. *Struct. Concr.* **2019**, *20*, 942–954. [CrossRef]
66. Bathe, K.-J.; Walczak, J.; Welch, A.; Mistry, N. Nonlinear analysis of concrete structures. *Comput. Struct.* **1989**, *32*, 563–590. [CrossRef]